TBK1 Knockdown Alleviates Axonal Transport Deficits in Retinal Ganglion Cells Via mTORC1 Activation in a Retinal Damage Mouse Model

Meng Ye,[1] Yuanyuan Hu,[1] Bowen Zhao,[1] Qianxue Mou,[1] Yueqi Ni,[1] Jing Luo,[2] Lu Li,[3,4] Hong Zhang,[1] and Yin Zhao[1]

[1]Department of Ophthalmology, Tongji Hospital, Tongji Medical College, Huazhong University of Science and Technology, Wuhan, People's Republic of China
[2]Institute of Reproductive Health, Center for Reproductive Medicine, Tongji Medical College, Huazhong University of Science and Technology, Wuhan, China
[3]Department of Ophthalmology, Affiliated Wuxi Clinical College of Nantong University, Wuxi, People's Republic of China
[4]Department of Ophthalmology, The Affiliated Wuxi No. 2 People's Hospital of Nanjing Medical University, Wuxi, People's Republic of China

Correspondence: Hong Zhang and Yin Zhao, Department of Ophthalmology, Tongji Hospital, Tongji Medical College, Huazhong University of Science and Technology, Wuhan 430030, People's Republic of China; tjyksys@163.com and zhaoyin85@hust.edu.cn.

MY and YH contributed equally to this work.

Received: November 4, 2022
Accepted: May 31, 2023
Published: July 3, 2023

Citation: Ye M, Hu Y, Zhao B, et al. TBK1 knockdown alleviates axonal transport deficits in retinal ganglion cells via mTORC1 activation in a retinal damage mouse model. *Invest Ophthalmol Vis Sci.* 2023;64(10):1. https://doi.org/10.1167/iovs.64.10.1

Purpose. Glaucoma is the leading cause of irreversible blindness worldwide and is characterized by progressive retinal ganglion cell (RGC) death and optic nerve degeneration. Axonal transport deficits are the earliest crucial pathophysiological changes in glaucoma. Genetic variation in the TANK-binding kinase 1 gene (*TBK1*) plays a role in the pathogenesis of glaucoma. This study was designed to investigate intrinsic factors underlying RGCs' damage and to explore the molecular mechanism of *TBK1* involvement in glaucomatous pathogenesis.

Methods. We established a mouse model of acute ocular hypertension and used *TBK1* conditional knockdown mice to investigate the role of *TBK1* in glaucoma. CTB-Alexa 555 was utilized to evaluate axonal transport in mice. To observe the efficiency of gene knockdown, we performed immunofluorescence staining. Immunoblotting and immunoprecipitation assays were performed to examine protein–protein colocalization. RT–qPCR was performed to measure the mRNA levels of Tbk1.

Results. In this study, we found that conditional TBK1 knockdown in RGCs resulted in increased axonal transport and protection against axonal degeneration. Through mechanistic studies, we found that TBK1 inhibited mTORC1 pathway activation by phosphorylating RAPTOR at Ser1189. Phosphorylation of RAPTOR at Ser1189 abrogated the interaction of RAPTOR with the deubiquitinase USP9X, leading to an increase in RAPTOR ubiquitination and a subsequent decline in protein stabilization.

Conclusions. Our study identified a novel mechanism involving an interaction between the glaucoma risk gene *TBK1* and the pivotal mTORC1 pathway, which may provide new therapeutic targets in glaucoma and other neurodegenerative diseases.

Keywords: glaucoma, axonal transport, neuroprotection, TBK1, mTORC1

Glaucoma is the leading cause of irreversible blindness worldwide and is characterized by progressive retinal ganglion cell (RGC) death and optic nerve degeneration.[1] Elevated intraocular pressure (IOP) is currently considered the most important and only controllable risk factor for glaucoma.[2] However, glaucoma is a multifactorial disease involving age, sex, genetics, and other factors.[3] Treatments aimed at lowering IOP are not always effective in preventing the progression of vision loss, and some patients present with glaucomatous optic nerve damage without elevated IOP.[2,4,5] Intrinsic factors underlying RGC damage are worth investigating. Neuronal injury in glaucoma can be mediated by multiple mechanisms, such as oxidative stress, axonal transport impairment, and neuroinflammation.[6] Molecular and cellular events associated with these pathological processes may be targets for inducing neuroprotection in glaucoma.

Genetic variation plays a role in the pathogenesis of glaucoma and indicates critical molecules associated with the disease. Gene copy number variation in the TANK-binding kinase 1 (*TBK1*) gene has been reported in normal tension glaucoma (NTG) cases.[7,8] *TBK1* gene duplication and triplication mutations on chromosome 12q14 results in a significant increase in the transcription level of *TBK1*, indicating its involvement in the progression of glaucoma pathology.[7] Transgenic *Tbk1* mice have been reported to exhibit features of glaucoma.[9] TBK1 is a serine–threonine kinase that phosphorylates and regulates the activity of multiple substrate proteins.[10] TBK1 regulates neuroinflammation and autophagy, the pathological processes associated with

neurodegenerative diseases.[11,12] Although TBK1 expression has been detected in the retinal ganglion cell layer,[13] the molecular mechanism of TBK1 involvement in glaucomatous pathogenesis is not yet fully understood.

The mammalian target of rapamycin (mTOR) pathway is the hub of intracellular metabolism and protein synthesis and thus plays an essential role in neural development and neuronal survival.[14,15] Dysfunction of the mTORC1 pathway is associated with many ocular neurodegenerative diseases.[16–18] A proteomic analysis of retina samples from patients with ocular hypertension and normotensive controls revealed significant proteomic alterations in the mTORC1 pathway of the patients.[19] Moreover, studies have suggested that activation of mTORC1 in RGCs may promote visual function, axonal transport, synaptic integrity, and axonal regeneration in glaucomatous mouse models.[20–22] These studies indicate a potential role for mTORC1 in neuroprotection against glaucoma.

The mTORC1 pathway is regulated by multiple mechanisms and engages in crosstalk with many other pathways. There is evidence that TBK1 interacts with mTORC1 in different ways in multiple cell types.[23-26] However, links between these two factors in neurodegenerative diseases, especially glaucoma, have not yet been explored. Considering the regulatory role and the potential relationship of these two proteins in glaucoma, we speculate that TBK1 may be involved in the pathogenesis of glaucoma by affecting the mTORC1 pathway activity.

In this study, we established a mouse model of acute ocular hypertension (AOHT) and used TBK1-conditional-knockdown mice to investigate the role of TBK1 in RGC damage. Our data suggested that TBK1 conditional knockdown in RGCs resulted in increased axonal transport and protection against axonal degeneration. Through mechanistic experiments, we found that TBK1 inhibited the mTORC1 pathway via the phosphorylation of RAPTOR, the key component of mTORC1, at Ser1189. Phosphorylation of RAPTOR on Ser1189 abrogated the interaction of RAPTOR with the deubiquitinase USP9X, leading to an increase in RAPTOR ubiquitination and a decline in subsequent protein stabilization. These findings reveal a novel association between TBK1 and mTORC1 and provides new insights into the involvement of TBK1 in glaucoma pathogenesis.

Materials and Methods

Animals

Tbk1$^{fl/fl}$ and *Rptor*$^{fl/fl}$ mice were obtained from the Jackson Laboratory. Adult male C57BL/6 mice were purchased from Gempharmatech (Nanjing, Jiangsu, China). All animals were housed in a specific pathogen-free (SPF) environment in the Animal Center of the Tongji Medical College. All these mice were maintained under a 12-hour light/dark cycle in a temperature and humidity-controlled room. All the animal operations were in accordance with ARVO Statement for the Use of Animals in Vision and Ophthalmic Research and the institutional IACUC committees of Huazhong University of Science and Technology.

Reagents and Antibodies

CTB-Alexa 555 was bought from BrainVTA (Wuhan, Hubei, China). Degrasyn and Amlexanox were purchased from MedChemExpress (Monmouth Junction, NJ, USA). Proteasome inhibitor MG132 (Calbiochem), cycloheximide (CHX; Sigma-Aldrich). Antibodies: anti-NAK/TBK1 (ab40676; Abcam); anti-NAK/TBK1 (ab109272; Abcam); anti-USP9X (ab180191; Abcam); anti-synaptophysin (ab14692; Abcam); anti-p70S6k (2708T; Cell Signaling Technology); anti-p-p70S6k (9234T; Cell Signaling Technology); anti-GAPDH (10494-1-AP; Proteintech);anti-HA (TT0008; Abmart); anti-GFP (M20004; Abmart); anti-MYC (M20002; Abmart); anti-His (M20001; Abmart); anti-Flag (TT0003; Abmart); anti-Flag (66008-4-Ig; Proteintech); anti-β-actin (sc-47778; Santa Cruz); anti-RAPTOR (20984-1-AP; Proteintech); anti-Tuj1 (801201; Biolegend); anti-Iba1 (ab48004; Abcam); anti-GAFP (ab4674; Abcam); and anti-pS6(Ser240/244) (5364T; Cell Signaling Technology).

Adeno-Associated Virus Administration

AAV2-hsyn-Cre-EGFP-WPRE-PA and AAV2-hsyn-EGFP-WPREPA were produced by GeneChem (Shanghai, China). Using a Hamilton microsyringe (Hamilton, Reno, NV, USA) with a 35G needle, each eye was intravitreally injected with 2 µL of AAV virus (approximately 2.0×10^{12} genome copies/mL). To allow for IOP equilibration, we kept the needle in place for 60 seconds before the withdrawal. Four weeks later, the mice were used for further experiments.

Animal Model of Acute Ocular Hypertension

The acute high IOP model was conducted according to previously described methods.[27] Briefly, the mice were deep anesthetized by intraperitoneal injection of 5% chloral hydrate (9 mL/kg). The pupils were dilated with 1% tropicamide followed by 0.5% tetracaine hydrochloride ophthalmic topical anesthetic solution. We used a 30-gauge needle, which was connected to a silicone infusion line of balanced salt solution to cannulate the anterior chamber of the eye under microscopic guidance; avoiding injury to the corneal endothelium, iris, and lens. We elevated the saline reservoir to a height of 1.2 m for 1 hour. We treated the left eye of the mouse with the AOHT/AAV model and the contralateral eye of each animal with a sham procedure served as a non-ischemic control. After removing the needle, antibiotic ointment was applied topically to prevent infection. The animals were euthanized at different time points after acute ocular hypertension.

Immunofluorescence

The eyes and optic nerve were fixed in 4% paraformaldehyde (PFA) at room temperature for 2 days and processed either for paraffin or frozen sectioning. For paraffin sections, the tissues were dehydrated, embedded in paraffin, and serial sections (4 µm) were generated. For frozen sections, the optic nerve was isolated from a distance of 1.5 mm from the proximal end of the globe, and then dehydrated in 30% sucrose for 24 hours, followed by being frozen with optimal cutting temperature compound (OCT) and produced 4 µm sections in a Leica CM1950 cryostat microtome.

The sections were gently washed three times with phosphate-buffered saline (PBS), permeabilized with 0.1% Triton X-100 for 30 minutes, blocked in 5% donkey serum albumin for 1 hour, and then incubated with primary antibodies at 4°C overnight, followed by appropriate secondary antibodies. Cells grown on glass coverslips were fixed with

Investigative Ophthalmology & Visual Science

4% paraformaldehyde for 15 minutes at room temperature, and immunofluorescence was prepared using the same protocol as for the sections (as above).

For retinal flat mount, eyes were dissected and fixed in 4% PFA for 2 hours at room temperature. Cutting the posterior segments of the eyes into a "petal" shape with four to five radial incisions, and then detaching the retinas carefully. We left the retinas in cold methanol for at least 20 minutes to facilitate permeabilization. The retinas were rinsed in PBS, blocked in normal donkey serum for 1 hour, and then incubated for 48 to 72 hours at 4°C with primary antibodies, followed by appropriate secondary antibodies at room temperature for 90 minutes. After that, the retinas were transferred onto slides and mounted with glycerol.

Images were captured using an inverted confocal microscope (Zeiss LSM 710; Zeiss, Oberkochen, Germany). Each optic nerve was selected 10 grids (200 µm * 200 µm) randomly, and the number of axonal swellings per unit area was measured using ImageJ software. Only those swellings over 5 µm in diameter were analyzed.[28] Colocalization analysis was performed by calculating Pearson's correlation coefficient using ImageJ software.

Evaluation of Anterograde Axon Transport by Cholera Toxin β-Subunit

Animals were anesthetized with 5% chloral hydrate and mydriatic with 1% tropicamide. CTB-Alexa 555 was intravitreally injected, 1.5 uL for one eye. Forty-eight hours later, the mice were anesthetized, and the hearts were perfused with 0.9% NaCl and 4% PFA in sequence, by cardiac intraventricular canalization. Then, the brains and eyes were post-fixed for 48 hours with 4% PFA, dehydrated with 30% sucrose overnight, followed by embedding in OCT (Tissue-Tek, Sakura Finetek Inc, Tokyo, Japan). Superior colliculus was continuously sliced into 30 µm sections. The eyes were sectioned into 8 µm with optic nerve head (ONH). Using a fluorescent microscope (Olympus, Tokyo, Japan) to get images. The distance of CTB labeling in ONH sections and the area of the CTB signal in each superior colliculus (SC) section were measured using ImageJ software.

Cell Culture and Transfection

HEK-293T cells were purchased from Boster Biologic Technology. SH-SY5Y cells were a gift from the Department of Neurobiology, Tongji Medical College, Huazhong University of Science and Technology. HEK-293T and SH-SY5Y cells were cultured in high-glucose DMEM (Hyclone Laboratories, Logan, UT, USA) supplemented with 10% FBS (Gibco, Anaheim, CA, USA) at 37°C with 5% CO2.

HEK-293T and SH-SY5Y cells were transfected with GFP-TBK1 (WT/K38A), Flag-RAPTOR (WT/1189A/1189D), Myc-USP9X plasmid/vehicle, and siTBK1 using Lipofectamine 3000 (Thermo Fisher Scientific) according to the transfection protocol. Cells were harvested for further analyses 48 hours after transfection. Sequence (5′ to 3′) of siTBK1: #1 5′-TCAAGAACTTATCTACGAA-3′; #2 5′-GACAGAAGUUGUGAUCACA-3′.

Neurite Outgrowth Assay

We used retinoic acid (RA; all-trans-retinoic acid; Sigma) to induce cell differentiation and neurite outgrowth. SH-SY5Y cells were seeded in 6-well plates, and exposed to 100 µM hydrogen peroxide for 8 hours to inhibit neurite outgrowth. After recovered in normal medium for another 12 hours, the cells were fixed in 4% PFA for 15 minutes, and then rinsed with PBS. Randomized images were acquired on a IX71 microscope (Olympus, Tokyo, Japan), mean neurite outgrowth was quantified in ImageJ software. The average length of the neurites was analyzed.

Protein Extraction, Immunoblot, and Immunoprecipitation

Cells and retina were lysed in RIPA buffer (Applygen Technologies, Beijing, China) supplemented with protease and phosphatase inhibitors (Boster Biologic Technology). The protein concentrations of lysates were determined with the BCA Protein Assay Reagent. Protein lysates were boiled with loading buffer (Boster Biologic Technology) for 5 minutes. The equivalent amounts of protein lysates were resolved by SDS-PAGE and transferred to polyvinylidene difluoride (PVDF) membranes (MilliporeSigma). Membranes were blocked with 5% non-fat dry milk in Tris-buffered saline-Tween 20 (TBST) and treated with primary antibody overnight at 4°C. For immunoprecipitation, the same amounts of whole-cell lysate were incubated with the primary antibodies (0.5−2 µg) overnight at 4°C, followed by added protein A/G sepharose beads (P2012; Beyotime Biotechnology) into the incubation tubes and then being incubated together at 4°C for 3 hours. The precipitated complexes were washed five times with RIPA buffer before being resolved by SDS-PAGE followed by immunoblot analysis with indicated antibodies.

Drug Administration

Retinoic acid (R2625; Sigma) powder was dissolved in DMSO at 3 mg/mL (0.01 M) as stock solution and stored at −80°C with light-protected vials. To induce differentiation of SH-SY5Y cells, we diluted the stock solution with a tissue culture medium at a final concentration of 10 µM.

For the construction of damage models in cellular experiments, we treated SH-SY5Y cells with H_2O_2 (50 µM). Cells were harvested and followed by subsequent experiments after being treated with H_2O_2 for 8 hours.

For cells, Amlexanox and Degrasyn were diluted in DMSO according to the manufacturer's instructions and then further diluted in complete cell culture media at a final concentration of 100 µM (Amlexanox) or 5 µM (Degrasyn). For animals, mice are randomly assigned to 2 groups: one group received Degrasyn (40 mg/kg, intraperitoneally) in 100 µL DMSO every 2 days (7 injections); and the other received DMSO (vehicle) every other day (7 injections). CHX (100 µg/mL) was used for protein stability assay and cells were harvested at different time points for the preparation of WCL and subsequent Western blot analysis.

RNA Isolation and Real-Time Quantitative PCR

RNA was extracted using RNAiso plus (Takara Biomedical Technology, Beijing, China), followed by the determination of RNA concentration. The reverse-transcription (RT) reaction was performed with PrimeScript RT reagent Kit (RR047A; Takara Biomedical Technology). The real-time quantitative PCR reaction was performed with TB

Investigative Ophthalmology & Visual Science

Green-Premix Ex Taq (RR420A; Takara Biomedical Technology) and a 7300 Real-Time PCR System (Applied Biosystems). All samples were run in triplicate with blank controls. The relative gene expression was calculated by the $2^{-\Delta\Delta CT}$ method with normalization against the Gapdh level.

Primer sequences were designed as follows:

Raptor: forward 5′-ACTGGAACCTACCTTTGGCTT-3′,
Reverse 5′-ACTGTCTTCATCCGATCCTTCA-3′,
Gapdh: forward 5′-GGAGTCCACTGGCGTCTTCA-3′, and
reverse 5′- GTCATGAGTCCTTCCACGATACC-3′.

Statistical Analysis

The experiments were repeated at least three times unless stated otherwise. The results were presented as mean ± SD of at least three biologically independent experiments or samples. Statistical analyses were performed in GraphPad Prism 7 and Excel. Statistical significance within the experimental groups was assessed by Student's *t*-test or 1-way analysis of variance (ANOVA). Any *P* value less than 0.05 was considered significant.

Results

Axon Transport Deficits Characterized Early Disease and the TBK1 Expression Pattern in the Retina in the AOHT Model

Axonal transport deficits have been implicated in axonal dysfunction and neurodegeneration in glaucoma.[29] First, we detected anterograde transport by intravitreal injection of the cholera toxin β-subunit (CTB), which is a neural tracer taken up by RGCs and transported along the optic nerve to the visual cortex. CTB signals in the optic nerve head (ONH) and SC were measured. The distance that the CTB label moved in the ONH (Fig. 1A) and the CTB projection in the SC (Fig. 1B) were clearly decreased on day 2. Synaptophysin, a marker of endogenous cargo transport, accumulated in the ONH after model establishment (Fig. 1C). These results indicated that axonal transport was blocked after AOHT was induced. Furthermore, immunofluorescence measurement of Tuj1 was performed to detect changes in axon morphology 0, 1, 3, 5, and 7 days after AOHT induction. Focal axonal swelling, characterized by the aggregation of organelles and cargo in axons, is generally regarded as an early sign of axonal degeneration.[30] The results of our experiment clearly showed increased axonal swelling on days 5 and 7 (Figs. 1D, 1E). Similarly, RGCs' evident loss was observed on day 7 (Figs. 1F, 1G). The axonal swelling and the number of RGCs in the sham-operated group are shown in the supplementary material (Supplementary Figs. S1A-D). In conclusion, axon transport impairment was the earliest crucial pathophysiological changes underlying axonal degeneration in the glaucoma model.[31]

As shown in Figure 1H, immunofluorescence staining showed that TBK1 expression was increased in the retina following AOHT induction. Moreover, a Western blot analysis revealed that TBK1 protein levels in the retina were increased (Figs. 1I, 1J). Protein levels of TBK1 were consistently elevated at 5 days after treatment in the AOHT model (see Supplementary Figs. 1E, 1F). To explore the cellular localization of TBK1 in the retina, we labeled both TBK1 with markers of RGCs (Tuj1), microglia (Iba1), and astrocytes (GAFP) with immunofluorescence dye (Figs. 1K–M). TBK1 colocalized with Tuj1, Iba1, and GFAP, but TBK1 expression was upregulated significantly only in the RGCs and microglia after AOHT induction. Therefore, we assumed that TBK1 might function mainly in RGCs and microglia during glaucoma pathogenesis.

TBK1 Knockdown in RGCs Prevented AOHT-Induced Axonal Transport Deficits and Neuronal Degeneration

To study the specific role played by TBK1 in RGCs, we generated TBK1-conditional knockdown mice by injecting AAV-hsyn-cre-EGFP into the vitreous body of *Tbk1*$^{fl/fl}$ mice (Fig. 2A). A schematic representation of the experimental results is shown in Supplementary Figure S2. To verify the efficiency and specificity of virus transfection, immunofluorescence staining of RBPMS and EGFP tags was performed. EGFP was clearly expressed in the AAV-Cre-EGFP and AAV-EGFP groups and was mainly localized in RGCs (Fig. 2B). TBK1 expression was significantly downregulated in the AAV-Cre-EGFP group (Fig. 2C). In an ONH tissue section, the CTB signal was clearly observed to have been recovered and the accumulation of synaptophysin was reduced after AOHT in the TBK1-knockdown mice (Figs. 2D, 2F, 2H). Moreover, TBK1 knockdown significantly increased the CTB signal in the SC after AOHT (see Figs. 2E, 2G). In addition, the axonal swelling induced by AOHT was effectively alleviated following TBK1 knockdown (Figs. 2I, 2J). The loss of RGCs caused by the AOHT model was also ameliorated by knocking down TBK1 within the RGCs (Fig. 2K). In summary, TBK1 knockdown in RGCs exerted neuroprotective effects on the AOHT model.

TBK1 Knockdown Protected Against Axonal Transport Deficits and Neuronal Degeneration Through an mTORC1-Dependent Mechanism

The mTOR signaling pathway is crucial for regulating neuronal function.[32] Evidence suggests that TBK1 and mTORC1 establish a mechanical link.[25] TBK1 can promote the phosphorylation of RAPTOR Ser877 and then inhibit mTORC1 activity.[24] These data suggest a potential interaction between mTORC1 and TBK1. To explore whether mTORC1 is involved in TBK1-mediated effects in AOHT, we examined mTORC1 activity. As shown in Figure 3A, phosphorylated S6 (p-S6) expression was decreased in the AOHT group, whereas TBK1 knockdown prevented this decline. To further explore the role of TBK1 in nerve cells, we treated SH-SY5Y cells, a neuroblastoma cell line, with H_2O_2 to imitate cell injury similar to that in retinal degeneration.[33] A Western blot analysis illustrated that the phosphorylated pS6K (p-pS6K) level was reduced after H_2O_2-induced injury (Figs. 3B–D). Furthermore, to verify the relationship between mTORC1 and TBK1, TBK1 siRNA was used, and the interference efficiency is shown in Figure 3E. The levels of p-pS6K were restored after TBK1 interference even after H_2O_2 treatment (Figs. 3F, 3G). In addition, we found that the neurite outgrowth inhibited by H_2O_2-induced injury was restored after TBK1 interference (Figs. 3H, I). Hence, the neuroprotective effect induced by TBK1 knockdown is mediated by an mTORC1-dependent mechanism.

An mTORC1 consists mainly of mTOR, mLST8, and RAPTOR. To identify the downstream targets of TBK1, we compared the protein levels of mTORC1 components

Investigative Ophthalmology & Visual Science

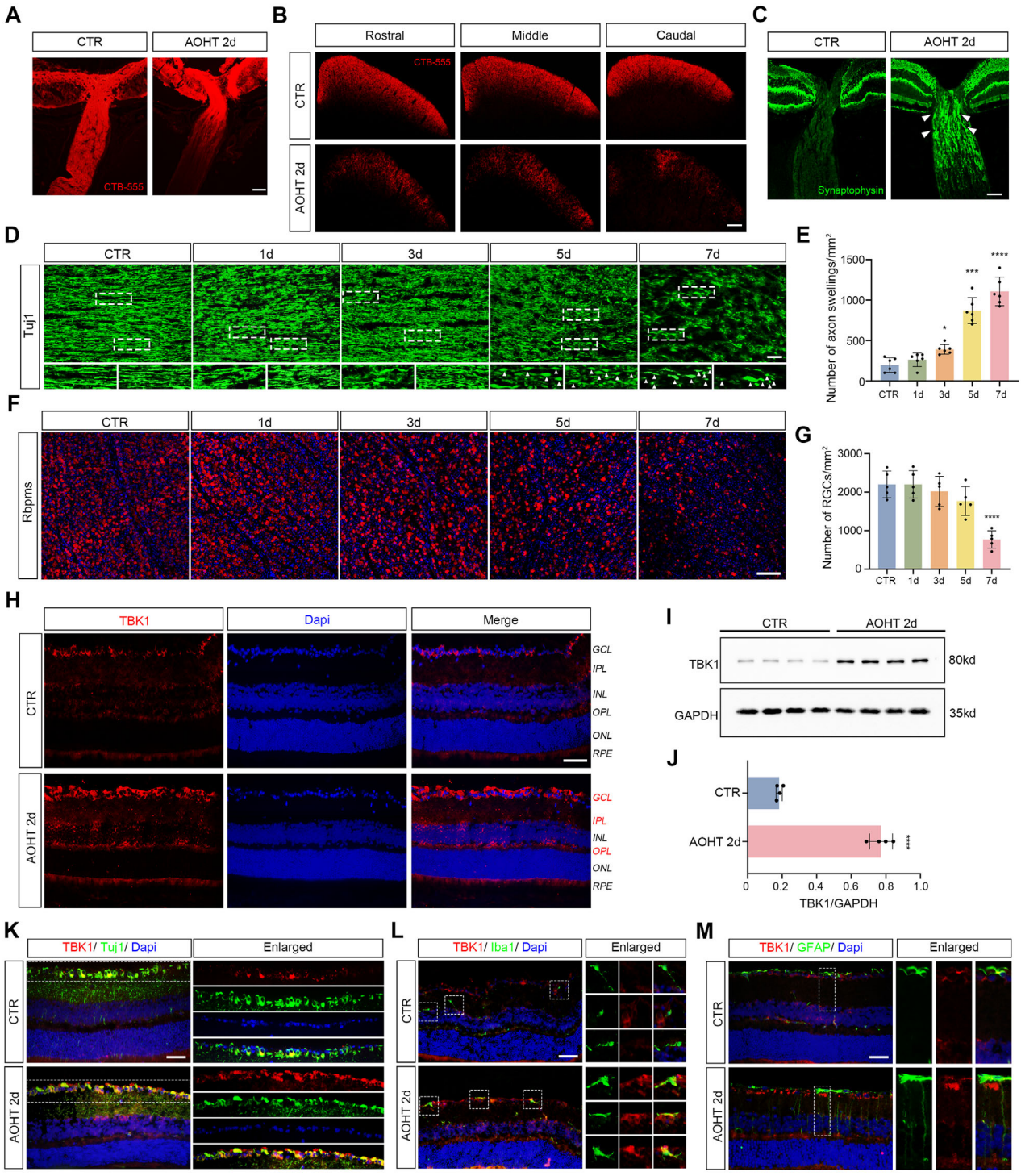

Figure 1. TBK1 expression was upregulated in retina after acute ocular hypertension (AOHT). (**A**) Representative images showing anterograde transport of CTB-555 in ONH and proximal ON in CTR and 2-day groups post-AOHT, $n = 6$ eyes/group. Scale bar = 50 µm. (**B**) Representative images of CTB-555 transported to SC in CTR and 2-day groups post-AOHT, 3 layers: rostral, middle, and caudal are shown, $n = 6$ brains. Scale bar = 200 µm. (**C**) Immunostaining of synaptophysin in ONH in the same groups as in **B**. Scale bar = 50 µm. *White arrowheads* indicate the accumulation of synaptophysin protein. (**D**) Immunostaining of Tuj1 in optic nerves in groups of CTR, 1 day, 3 days, 5 days, and 7 days post AOHT. *White arrowheads* indicate the axon swellings, $n = 6$ optic nerves/group. Scale bar = 20 µm. (**E**) Statistical analysis of the number of axon swellings indicated in **D**, $n = 6$ optic nerves, 1-way ANOVA. (**F**) Immunostaining of RBPMS in the retinal flat mounts in the same groups as in **D**, $n = 5$ eyes/group. Scale bar = 100 µm. (**G**) Statistical analysis of the data shown in **F**, $n = 5$ eyes. (**H**) Immunofluorescence staining of TBK1 in retina of CTR and 2-day groups post-AOHT. Nuclei were detected by DAPI staining, $n = 6$ eyes/group. Scale bar = 50 µm. (**I**) Western blot analysis showing the protein level of TBK1 in mouse retina at 2 days after AOHT, $n = 4$ eyes/group. (**J**) Statistical analysis of the data shown in **I**, $n = 4$ eyes/group. (**K-M**) Co-immunofluorescent staining of TBK1 (*red*) with RGC marker Tuj1 (*green*) **K**, microglia marker Iba1 (*green*) **L**, astrocyte marker (GFAP) **M** in mouse retina of CTR and 2d groups following AOHT, $n = 5$ eyes/group. Scale bar = 50 µm. The data in **E**, **G**, and **J** were expressed as mean ± SD, 1-way ANOVA $^{*}P < 0.05$, $^{***}P < 0.001$, $^{****}P < 0.0001$.

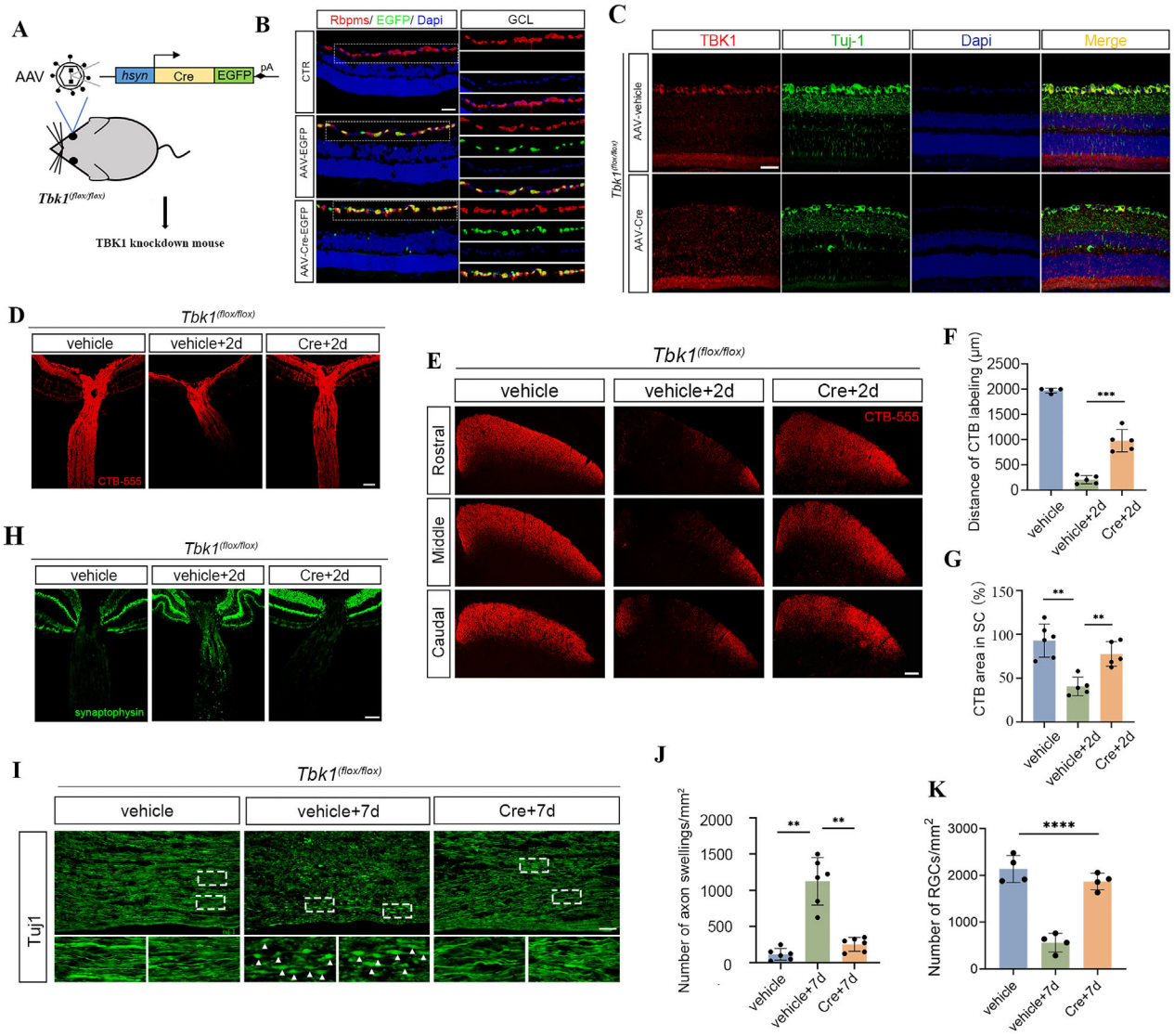

Figure 2. Knockdown of TBK1 prevented axonal transport deficits and neuronal degeneration from AOHT. (**A**) A schematic representation of the recombined adeno-associated virus (rAAV) construction and AAV injection into the transgenic mouse. (**B**) Representative images showing the transfection efficiency of the rAAV in retina. RGCs were marked with RBPMS (*red*). The expression of the EGFP tag was induced by hsyn promoter. Nuclei were detected by DAPI staining, $n = 4$ eyes/group. Scale bar = 50 μm. (**C**) Representative images showing the knockdown efficiency of TBK1 in retina. RGCs and nerve fibers were marked with Tuj1 (*green*). Nuclei were detected by DAPI staining, $n = 4$ eyes/group. Scale bar = 50 μm. (**D**) Representative images showing anterogradely transported of CTB-555 in ONH and proximal ON with or without TBK1 knockdown after AOHT, in the vehicle group $n = 4$ eyes, in the other groups $n = 5$ eyes/group. Scale bar = 50 μm. (**E**) Representative images of CTB-555 signal in SC in vehicle and 2 day groups with or without TBK1 knockdown post-AOHT, 3 layers: rostral, middle, and caudal were shown, $n = 5$ brains/group. Scale bar = 200 μm. (**F**) Statistical analysis of the CTB labeling distance shown in **D**, in the vehicle group $n = 4$ eyes, in the other groups $n = 5$ eyes/group. (**G**) Statistical analysis of CTB area shown in **E**, $n = 5$ brains/group. (**H**) Immunostaining of synaptophysin in ONH in the same groups as in **D**, $n = 5$ eyes/group. Scale bar = 50 μm. (**I**) Immunostaining of Tuj1 in the optic nerve at 7 days after AOHT, $n = 6$ optic nerves/group. *White arrowheads* indicate the axon swellings. Scale bar = 20 μm. (**J**) Statistical analysis of the number of axon swellings indicated in **I**, $n = 6$ optic nerves/group. (**K**) Statistical analysis of the number of RGCs, $n = 4$ RGCs/group. The data in **F**, **G**, **J**, and **K** were expressed as mean ± SD, 1-way ANOVA, $^{**}P < 0.01$, $^{***}P < 0.001$, $^{****}P < 0.0001$.

in H_2O_2-treated cells. Interestingly, the protein levels of RAPTOR were downregulated in the H_2O_2-treated cells but were restored after siTBK1 transfection (Figs. 3J, 3K). Furthermore, the RAPTOR protein levels clearly declined after TBK1 was overexpressed (Figs. 3M, 3N). Moreover, the reduction in the RAPTOR level in RGCs resulting from AOHT was restored in TBK1-knockdown mice. (Fig. 3L). As shown in Figure 3M, mTORC1 activity was suppressed following TBK1 overexpression, and this effect was blocked after RAPTOR supplementation (Figs. 3O, 3P). These results indicated that mTORC1 inactivation by TBK1 overexpression was due to the downregulation of RAPTOR.

The Neuroprotective Effect of TBK1 Knockdown Was Mediated by RAPTOR

To confirm that the mTORC1-dependent mechanism of TBK1 knockdown was mediated by RAPTOR, we generated TBK1-/RAPTOR-double-knockdown mice (Fig. 4A).

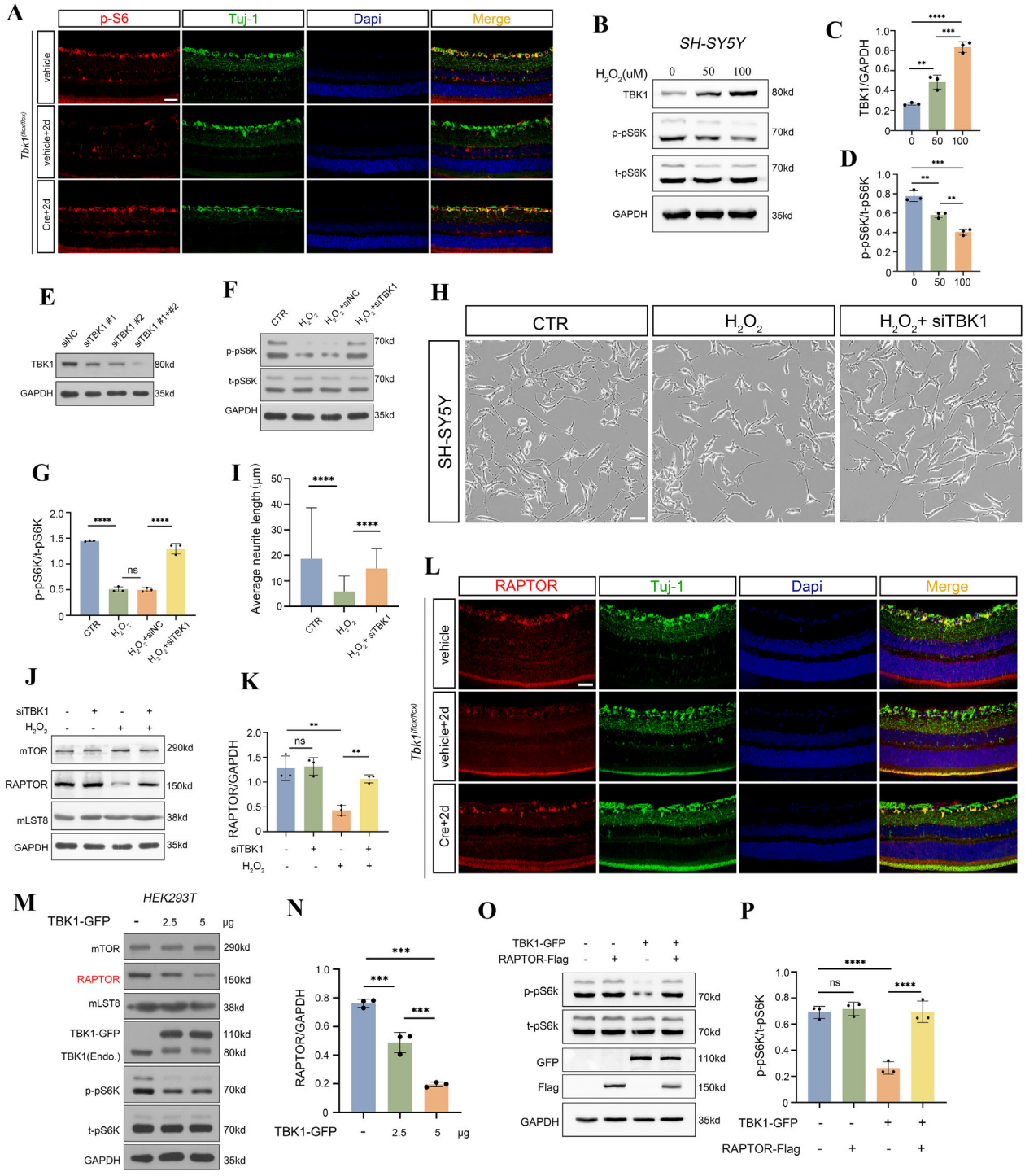

Figure 3. Knockdown of TBK1 protected against axonal transport deficits and neuronal degeneration through mTORC1-dependent mechanism. (**A**) Co-immunofluorescent staining of p-S6 (*red*) and Tuj1 (*green*) in *Tbk1*$^{fl/fl}$ mice with AAV-vehicle or AAV-Cre injection at 2 days after AOHT, nuclei were detected by DAPI staining, $n = 6$ eyes/group. Scale bar = 50 μm. (**B**) Western blot analysis of TBK1 and p-pS6K in SH-SY5Y cells with or without H_2O_2 (50 or 100 μM) treatment. (**C, D**) Statistical analysis of the data shown in **B**. (**E**) Western blot analysis of TBK1 with small interfering RNA (siRNA) transfection in SH-SY5Y cells. (**F**) Western blot analysis of p-pS6K with or without TBK1 siRNA after H_2O_2 (50 μM) treatment in SH-SY5Y cells. (**G**) Statistical analysis of the data shown in **F**. (**H**) Representative images showing neurite outgrowth of SH-SY5Y cells. Cells were treated with 50 μM H_2O_2 with or without TBK1 siRNA. Scale bar = 20 μm. (**I**) Statistical analysis of the neurite length shown in **H**. Twenty nonoverlapping fields were selected for analysis in each group from at least three experiments, $n = 200$ cells. (**J**) Western blot analysis of mTOR, RAPTOR, and mLST8 in SH-SY5Y cells. Cells were treated with 50 μM H_2O_2 with or without TBK1 siRNA. (**K**) Statistical analysis of RAPTOR protein level shown in **J**. (**L**) Representative images showing co-immunofluorescent staining of RAPTOR (*red*) and Tuj1 (*green*) in *Tbk1*$^{fl/fl}$ mice with the injection of AAV-vehicle or AAV-Cre at 2 days after AOHT, $n = 6$ eyes/group. Scale bar = 50 μm. (**M**) Western blot analysis of RAPTOR and p-pS6K in HEK-293T cells transfected with TBK1-GFP overexpression plasmids. (**N**) Statistical analysis of RAPTOR protein levels in **M**. (**O**) Western blot analysis of p-pS6K in HEK-293T cells co-transfected with TBK1-GFP and RAPTOR-Flag. (**P**) Statistical analysis of the data shown in **O**. Statistical tests in **C**, **D**, **G**, **I**, **K**, **N**, and **P** using 1-way ANOVA, $^{**}P < 0.01$, $^{***}P < 0.001$, $^{****}P < 0.0001$, ns, not statistically significant.

Investigative Ophthalmology & Visual Science

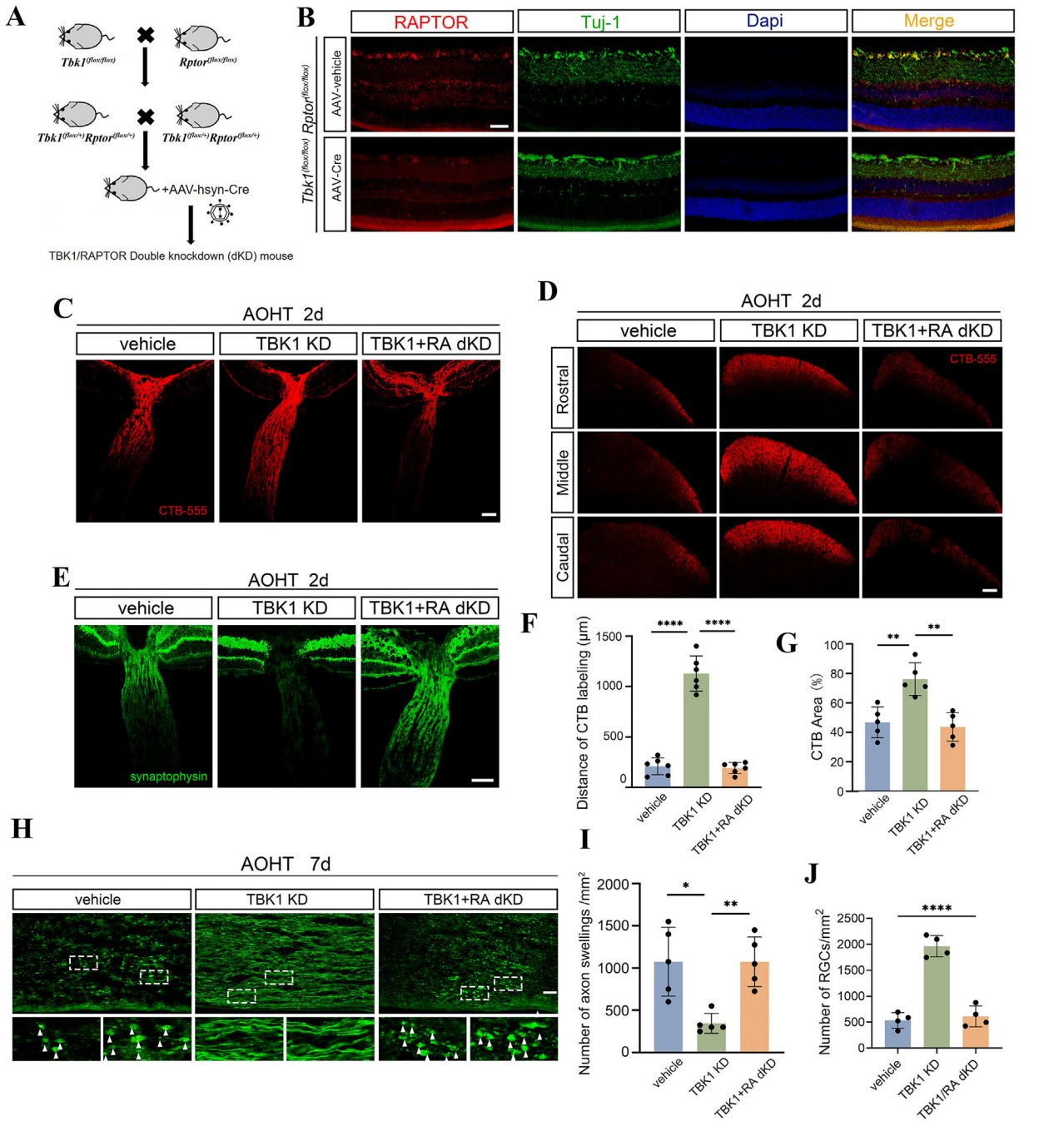

Figure 4. Knockdown of RAPTOR attenuated the neuroprotective effect of TBK1 knockdown. (**A**) Schematic diagram showing the generation of the TBK1/RAPTOR conditionally double-knockdown (dKD) mice. (**B**) Co-immunofluorescent staining of RAPTOR (*red*) and Tuj1 (*green*) showing the knockdown efficiency of RAPTOR in retina of $Tbk1^{fl/fl}$ $Rptor^{fl/fl}$ mice with injection of AAV-vehicle or AAV-Cre. Scale bar = 50 μm. (**C**) Representative images showing anterogradely transported CTB-555 in ONH and proximal ON in TBK1 and RAPTOR double-knockdown (dKD) mice after AOHT, $n = 6$ eyes/ group. Scale bar = 50 μm. (**D**) Representative images of CTB-555 signal in SC in the same groups as in **C**, 3 layers: rostral, middle, and caudal were shown, $n = 5$ brains/ group. Scale bar = 200 μm. (**E**) Immunostaining of synaptophysin in ONH in the same groups as in **C**, $n = 6$ eyes/ group. Scale bar = 50 μm. (**F**) Statistical analysis of the CTB labeling distance shown in **C**. The data were expressed as mean ± SD, $n = 6$ eyes/ group, 1-way ANOVA, $^{****}P < 0.0001$. (**G**) Statistical analysis of the CTB area shown in **D**. Data were expressed as mean ± SD, $n = 5$ brains/ group, 1-way ANOVA, $^{**}P < 0.01$. (**H**) Immunostaining of Tuj1 in the optic nerve at 7 days following AOHT, $n = 5$ optic nerves/ group. *White arrowheads* indicate the axon swellings. Scale bar = 20 μm. (**I**) Statistical analysis of the number of axon swellings indicated in **H**. (**J**) Statistical analysis of the number of RGCs. The data were expressed as mean ± SD, $n = 5$ optic nerves/ group, 1-way ANOVA, $^{*}P<0.05$, $^{**}P < 0.01$, $^{****}P < 0.0001$.

The knockdown efficiency of RAPTOR in RGCs is shown in Figure 4B. The facilitation of axonal transport by TBK1 knockdown was blocked after RAPTOR knockdown (Figs. 4C–G). In addition, axonal integrity was disrupted, the number of swollen axons and the loss of RGCs was increased in the TBK1-/RAPTOR-double-knockdown mice compared with that in the TBK1-knockdown mice (Figs. 4H–J). Thus, RAPTOR was found to be necessary for the neuroprotective effect exerted by TBK1 knockdown.

TBK1 Suppressed mTORC1 by Inducing the Ubiquitination and Degradation of RAPTOR

Because the mRNA levels of RAPTOR did not change after TBK1 overexpression (Fig. 5A), the TBK1-induced decrease in RAPTOR protein levels may have been due to its reduced synthesis or increased degradation. Next, we performed a half-life experiment and found that TBK1 overexpression promoted the degradation of RAPTOR after cyclohexane treatment, which can inhibit protein synthesis (Figs. 5B, 5C). Autophagy and the proteasome system are two critical protein degradation systems in cells. We used the proteasome inhibitor MG132 and the lysosome inhibitor chloroquine to identify possible degradation pathways. Western blot assays showed that RAPTOR downregulation induced by TBK1 overexpression was prevented by MG132 treatment but did not respond to chloroquine treatment (Fig. 5D). Moreover, the levels of ubiquitinated RAPTOR were substantially increased after TBK1-GFP transfection (Fig. 5E) but were reduced after TBK1 siRNA transfection (Fig. 5F). These data demonstrated that the degradation of RAPTOR induced by TBK1 was related to the ubiquitin–proteasome degradation pathway.

Because TBK1 is a serine-threonine kinase, we wondered whether TBK1-mediated RAPTOR degradation is associated with its kinase activity. The phosphokinase activity of TBK1 was suppressed by amlexanox. As shown in Figure 5G, the downregulation of RAPTOR induced by H_2O_2 was restored with increasing doses of amlexanox. Furthermore, we found that transfection of wild-type TBK1-GFP, but not kinase-dead mutant TBK1(K38A), resulted in RAPTOR downregulation (Figs. 5H, 5I). Additionally, the ubiquitination levels of RAPTOR were abolished after TBK1-K38A overexpression (Fig. 5J), and its stability in the TBK1-K38A transfection group was better than that in the TBK1-WT transfection group (Figs. 5K, 5L). Collectively, these results emphasized the essential role of TBK1 kinase activity in the ubiquitination-mediated degradation of RAPTOR.

RAPTOR Ubiquitination-Related Degradation Was a Result of TBK1-Mediated RAPTOR Ser1189 Phosphorylation

Considering the role of TBK1 kinase activity in RAPTOR degradation, we explored whether phosphorylation was critical to the degradation of RAPTOR. Co-immunoprecipitation experiments were performed to evaluate the interaction of TBK1 and RAPTOR. The data showed that binding of the endogenous TBK1 and RAPTOR proteins (Figs. 6A, 6B). The phosphorylation levels of RAPTOR were increased after TBK1 overexpression (Figs. 6C, 6D). This result suggested that RAPTOR might be phosphorylated by TBK1. Next, we predicted the potential phosphorylation sites of RAPTOR that aligned with the TBK1 substrate motif using Group Based Prediction System 5.0 and PhosphoSite (www.phosphosite.org). The intersection of the predicted results is shown in Figure 6E. Considering these results, we constructed point-mutated plasmids via the site-directed mutation to replace an Ser residue with an Ala residue, which prevented phosphorylation. The RAPTOR-S1189A mutant abrogated the downregulation of RAPTOR that had been induced by TBK1 overexpression (Figs. 6F, 6G). Additionally, RAPTOR-S1189A diminished the TBK1-mediated phosphorylation of RAPTOR (Figs. 6H, 6I). The degradation of RAPTOR caused by TBK1 overexpression was not evident in the RAPTOR-S1189A mutant (Figs. 6J, 6K), as the mutation prevented the ubiquitination of RAPTOR mediated by TBK1 overexpression (Fig. 6L). In contrast, the phosphomimetic mutation S1189D promoted RAPTOR degradation (Figs. 6M, 6N) by increasing RAPTOR ubiquitination (Fig. 6O). In summary, TBK1 phosphorylates RAPTOR at Ser1189 and reduces RAPTOR protein stability via the ubiquitin–proteasome pathway.

RAPTOR Phosphorylation Increased RAPTOR Ubiquitination by Decreasing Its Interaction With USP9X

We next explored the molecular mechanisms underlying phosphorylation-dependent RAPTOR ubiquitination. A previous study had indicated that USP9X acted as a deubiquitylating enzyme and stabilized RAPTOR in neural progenitors.[34] In addition, USP9X was also reported to regulate axonogenesis[35] and neurodevelopment.[36] To explore the role of UAP9X in RAPTOR stabilization, we conducted co-immunoprecipitation experiments and confirmed the interaction between RAPTOR and USP9X (Figs. 7A, 7B), which was impaired by TBK1 overexpression (Figs. 7C, 7D). Furthermore, a colocalization analysis showed that the interaction between USP9X and RAPTOR was weaker after TBK1 was overexpressed (Figs. 7E, 7F). Subsequently, we found that the interaction USP9X and RAPTOR was not affected by a kinase-inactivation mutation in TBK1 (K38A) (Figs. 7G, 7H). In addition, the dephosphorylated mutant RAPTOR-S1189A bound more strongly to USP9X-Myc, whereas the phosphomimetic mutant RAPTOR-S1189D showed a weaker interaction with USP9X-Myc. (Figs. 7I, 7J). These results were confirmed via a colocalization analysis (Figs. 7K, 7L). To further explore the relationship between USP9X and RAPTOR degradation, degrasyn, which can suppress USP9X deubiquitinase activity, was used in an experiment. The reduction in RAPTOR degradation caused by interference with TBK1 activity was clearly inhibited by degrasyn (Figs. 7M, 7N). Furthermore, differences in ubiquitination levels in different states of RAPTOR-S1189 phosphorylation disappeared after degrasyn treatment (Fig. 7O). These data suggested that the phosphorylation status of RAPTOR S1189 affects the binding of USP9X to RAPTOR and thus reduces the stability of RAPTOR.

The Neuroprotection Conferred by TBK1 Knockdown Was Reversed by a USP9X Inhibitor

To evaluate the role of USP9X in vivo, degrasyn was used to treat TBK1-knockdown mice. Immunofluorescence staining revealed that USP9X was stably expressed in mouse RGCs (Fig. 8A). We found that RAPTOR upregulation caused by TBK1 knockdown was clearly attenuated by degrasyn

Investigative Ophthalmology & Visual Science

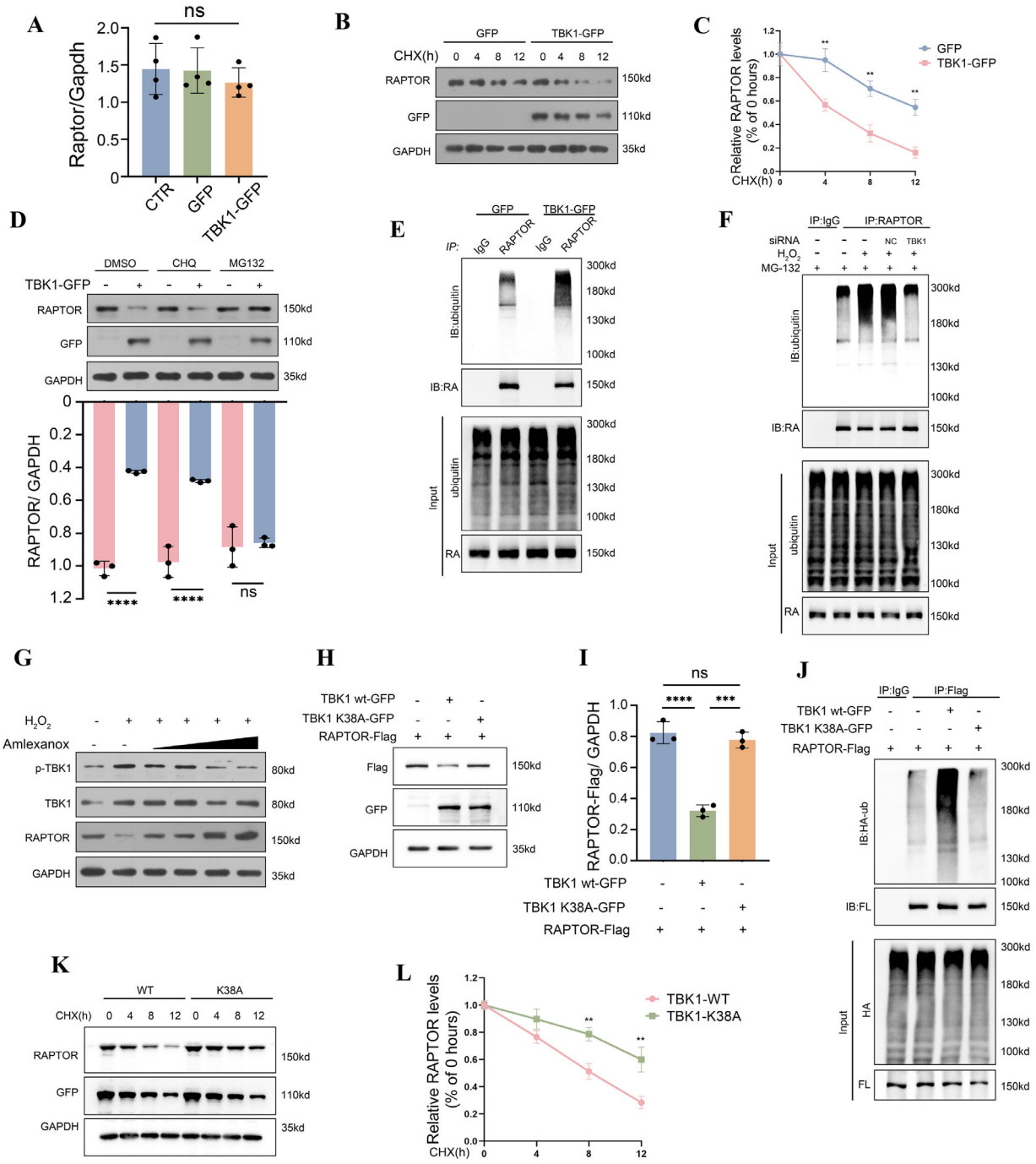

Figure 5. TBK1 suppressed mTORC1 via inducing the ubiquitination degradation of RAPTOR. (**A**) RT-PCR analysis of RAPTOR mRNA levels in HEK-293T cells. Cells were transfected with GFP or TBK1-GFP, $n = 4$. (**B**) Western blot analysis of RAPTOR protein half-life. HEK-293T cells were transfected with GFP or TBK1-GFP under CHX (protein synthesis inhibitor, 100 µg/mL) treatment. (**C**) Statistical analysis of the data indicated in **B**, $n = 3$. (**D**) Western blot analysis of RAPTOR protein levels (*upper panels*) in HEK-293T cells treated by DMSO, CHQ (lysosomal inhibitor, 10 µM), or MG132 (proteasomal inhibitor, 10 µM) with or without TBK1-GFP transfection. *Lower panels* showing statistical analysis of the data, $n = 3$. (**E**) Immunoprecipitation of ubiquitination with RAPTOR. HEK-293T cells were transfected with GFP or TBK1-GFP, $n = 3$. (**F**) Immunoprecipitation of ubiquitination with RAPTOR in SH-SY5Y cells under H_2O_2 (50 µM) treatment with or without TBK1 siRNA. (**G**) Western blot analysis of RAPTOR protein levels in SH-SY5Y cells treated with H_2O_2 (50 µM) and TBK1 inhibitor Amlexanox (gradient concentrations). (**H**) Western blot analysis of RAPTOR-Flag protein levels in HEK-293T cells. The cells were co-transfected with RAPTOR-Flag and TBK1 wild-type or TBK1 K38A (a kinase dead mutant). (**I**) Statistical analysis of the data indicated in **H**. (**J**) Immunoprecipitation of HA-ubiquitination with RAPTOR-Flag. The cells were treated as in **H**. (**K**) Western blot analysis of RAPTOR protein half-life. HEK-293T cells were transfected with TBK1 wild-type or TBK1 K38A under CHX treatment. (**L**) Statistical analysis of the data indicated in **K**. Data are presented as mean ± SD. Statistical tests for these data were performed using independent samples *t*-tests or 1-way ANOVA, $^{**}P < 0.01$, $^{***}P < 0.001$, $^{****}P < 0.0001$, ns, not statistically significant.

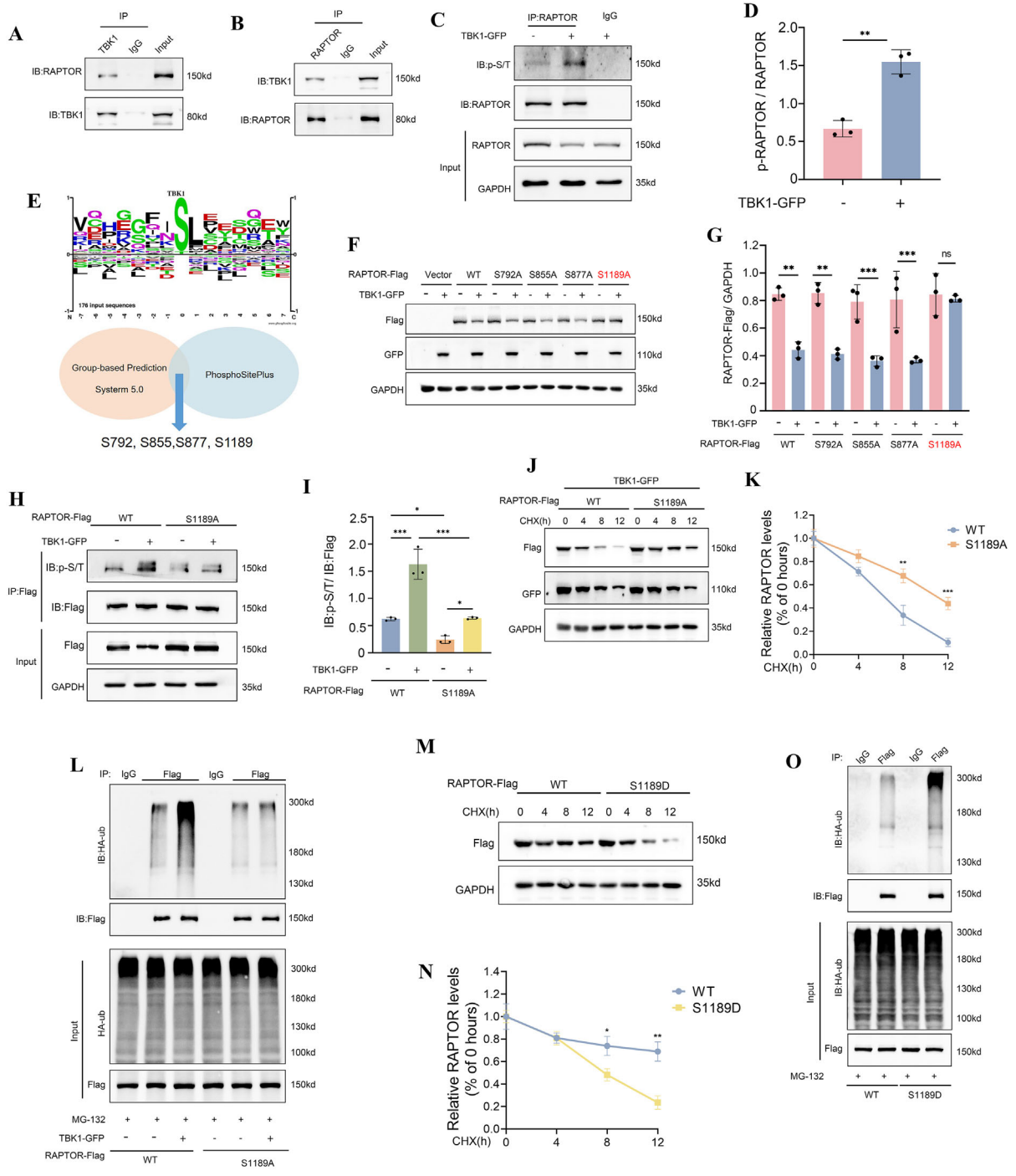

Figure 6. RAPTOR ubiquitination degradation resulted from RAPTOR Ser1189 phosphorylation mediated by TBK1. (**A, B**) Endogenous interaction between RAPTOR and TBK1 in mouse retina tissue lysates. (**C**) Immunoprecipitation of phosphorylated serine/threonine (p-S/T) with RAPTOR. HEK-293T cells were transfected with or without TBK1-GFP. (**D**) Statistical analysis of RAPTOR phosphorylation levels as shown in **C**. (**E**) Prediction of the potential sites in RAPTOR phosphorylated by TBK1 through intersection analysis of multi data base. (**F**) Western blot analysis of RAPTOR-Flag protein levels in HEK-293T cells transfected with RAPTOR-Flag wild-type or plasmids containing dephosphorylated mutation of Ser to Ala (S792A, S855A, S877A, and S1189A) with or without TBK1-GFP. (**G**) Statistical analysis of the data indicated in **F**. (**H**) Immunoprecipitation of phosphorylated serine/threonine (p-S/T) with RAPTOR-Flag. HEK-293T cells were transfected with RAPTOR-Flag wild-type or RAPTOR-Flag (S1189A) with or without TBK1-GFP. (**I**) Statistical analysis of the data indicated in **H**. (**J**) Western blot analysis of RAPTOR-Flag protein half-life. HEK-293T cells were co-transfected with TBK1-GFP and RAPTOR-Flag wild-type, or RAPTOR-Flag (S1189A). (**K**) Statistical analysis of the data indicated in **J**. (**L**) Immunoprecipitation of HA-ubiquitin with RAPTOR-Flag. HEK-293T cells were treated with MG132 following transfection of RAPTOR-Flag wild-type or RAPTOR-Flag (S1189A) with or without TBK1-GFP. (**M**) Western blot analysis of RAPTOR-Flag protein half-life. HEK-293T cells were transfected with RAPTOR-Flag wild-type or the phosphomimetic mutation S1189D. (**N**) Statistical analysis of the data indicated in **M**. (**O**) Immunoprecipitation of HA-ubiquitin with RAPTOR-Flag. HEK-293T cells were treated in MG132 following transfection of RAPTOR-Flag wild-type or RAPTOR-Flag (S1189D). Data were presented as mean ± SD. Statistical tests for these data were performed using independent samples *t*-tests or 1-way ANOVA, $^{**}P < 0.01$, $^{***}P < 0.001$, ns, not statistically significant. $^{***}P < 0.001$.

Investigative Ophthalmology & Visual Science

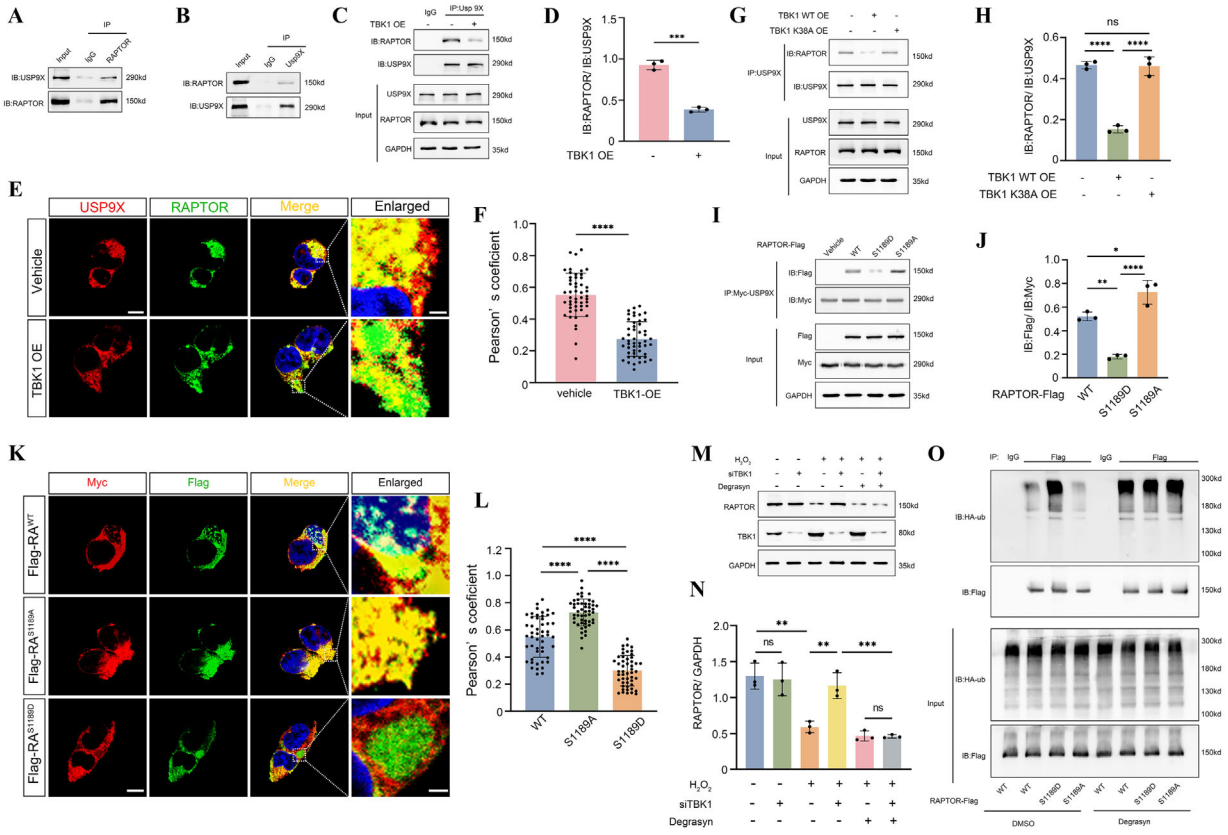

Figure 7. RAPTOR stability was regulated by Ser1189 phosphorylation via impacting its combination with the USP9X. (**A, B**) Endogenous interaction between RAPTOR and USP9X in mouse retina tissue lysates. (**C**) Co-immunoprecipitation of USP9X and RAPTOR in HEK-293T cells transfected with or without TBK1-GFP. (**D**) Statistical analysis of the data indicated in **C**. (**E**) Representative confocal images showing co-localization of USP9X and RAPTOR. Scale bar = 10 µm for the low-power fields and 2 µm for the high-power fields. (**F**) The Pearson's coefficient of the two channels in **E**. (**G**) Co-immunoprecipitation of RAPTOR with USP9X in HEK-293T cells. The cells were transfected with TBK1-GFP wild-type or TBK1-GFP containing a kinase dead mutation (K38A). (**H**) Statistical analysis of the data indicated in **G**. (**I**) Co-immunoprecipitation of wild-type or point mutation of RAPTOR with USP9X in HEK-293T cells. (**J**) Statistical analysis of the data indicated in **I**. (**K**) Representative confocal images showing co-localization of Myc-USP9X and RAPTOR-Flag. HEK-293T cells were co-transfected with Myc-USP9X and wild-type or point mutation RAPTOR-Flag. Scale bar = 10 µm for the low-power fields and 2 µm for the high-power fields. (**L**) Statistical analysis of the co-localization indicated in **K**. (**M**) Western blot analysis of RAPTOR protein levels in SH-SY5Y cells treated with USP9X inhibitor Degrasyn (5 µM) with or without TBK1 siRNA. (**N**) Statistical analysis of the data indicated in **M**. (**O**) Immunoprecipitation of HA-ubiquitin with RAPTOR-Flag. HEK-293T cells were transfected with RAPTOR-Flag wild-type or RAPTOR-Flag (S1189A) or RAPTOR-Flag (S1189D) with or without Degrasyn (5 µM). Data are presented as mean ± SD, 1-way ANOVA, $*P < 0.05$, $**P < 0.01$, $***P < 0.001$, $****P < 0.0001$, ns, no statistically significant.

after AOHT induction (Fig. 8B). The improvement of axonal transport by TBK1 knockdown was significantly abrogated by degrasyn (Figs. 8C–G). Moreover, swollen axons were observed after degrasyn treatment (Figs. 8H, 8I). In addition, the number of RGCs was significantly reduced after treatment with the USP9X inhibitor degrasyn, that is, the protective effect against axonal degeneration produced by knockdown of TBK1 within RGCs was lost (Fig. 8J). These results indicated the involvement of USP9X in controlling RAPTOR stabilization mediated by TBK1 knockdown and in conferring neuroprotective effects.

Discussion

Genetic studies have revealed that *TBK1* gene duplication is associated with NTG.[37] This copy number variation results in an elevated *TBK1* transcript level, suggesting a TBK1 gain-of-function mutation underlying glaucoma.[7,38] This mechanism was found to be independent of IOP, indicating that TBK1 might be associated with an intrinsic factor in RGCs during the pathogenesis of glaucoma. In our study, we measured TBK1 expression levels in the retina following AOHT induction and found a specific increase in the TBK1 expression of RGCs and microglia. This expression pattern indicated a possible multiregulatory function of TBK1 in different cells. TBK1 is considered to play a key role in neuroinflammation.[11,39] Mathur et al. showed that the STING-TBK1 pathway regulated microglial activity and neuroinflammation.[40] Xu et al. reported that TBK1 deficiency resulted in microglial activation and promoted neuroinflammation.[41] Considering the potential involvement of neuroinflammation in glaucoma, we suggest that TBK1 might play a role in microglia and indirectly participate in the pathogenesis of glaucoma. Thus, we established a conditional knockdown mouse model to explore the specific role of TBK1 in RGCs without affecting the level of TBK1 in microglia. The results showed that specific downregulation of TBK1 expression in RGCs via genetic methods effectively mitigated the development of the glaucoma phenotype.

The exact mechanism of TBK1 involvement in glaucoma pathogenesis has been extensively explored but has not

Investigative Ophthalmology & Visual Science

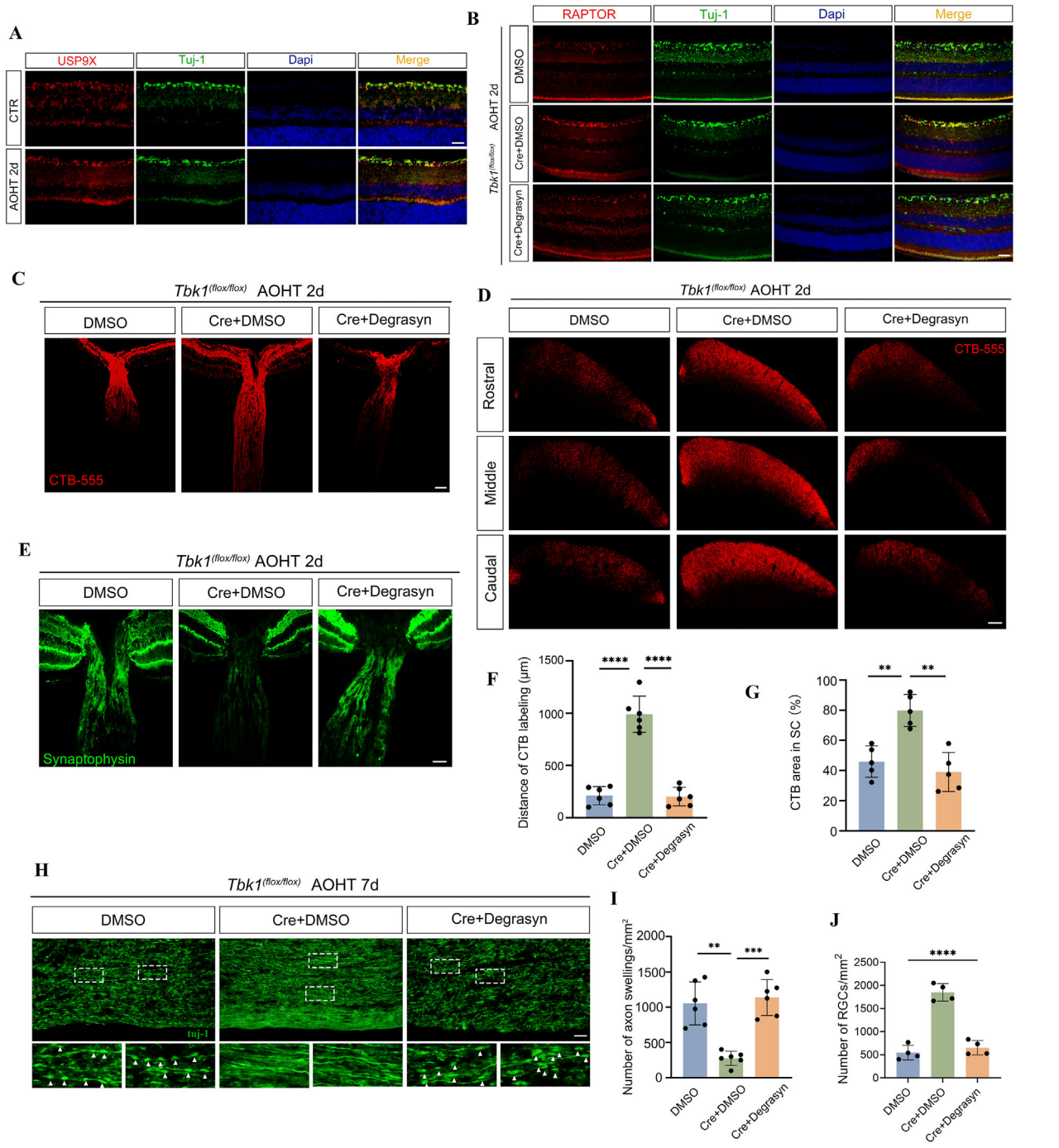

Figure 8. The neuroprotection effect of TBK1 knockdown was reversed by USP9X inhibition. (**A**) Representative images showing USP9X in mouse retina, nuclei were detected by DAPI staining. Scale bar = 50 μm. (**B**) Immunofluorescent staining of RAPTOR in mouse retina following TBK1 knockdown with or without Degrasyn (USP9X inhibitor) treatment after AOHT, nuclei were detected by DAPI staining, $n = 5$ eyes/group. Scale bar = 50 μm. (**C**) Representative images showing anterogradely transported CTB-555 in ONH and proximal ON following TBK1 knockdown with or without Degrasyn treatment after AOHT model, $n = 6$ eyes/group. Scale bar = 50 μm. (**D**) Representative images of CTB-555 transported to SC in the same groups as in **C**, 3 layers: rostral, middle, and caudal were shown, $n = 5$ brains/ group. Scale bar = 200 μm. (**E**) Immunostaining of synaptophysin in ONH in the same group as in **C**, $n = 6$ eyes/group. Scale bar = 50 μm. (**F**) Statistical analysis of the CTB labeling distance shown in **C**. The data were expressed as mean ± SD, $n = 6$ eyes/group, 1-way ANOVA, $^{****}P < 0.0001$. (**G**) Statistical analysis of CTB area shown in **D**. Data were expressed as mean ± SD, $n = 5$ brains/group, 1-way ANOVA, $^{**}P < 0.01$. (**H**) Immunostaining of Tuj1 in the optic nerve at 7 days following AOHT, $n = 6$ optic nerves/group. *White arrowheads* indicated the axon swellings. Scale bar = 20 μm. (**I**) Statistical analysis of the number of axon swellings indicated in **H**. (**J**) Statistical analysis of the number of RGCs. The data were expressed as mean ± SD, $n = 6$ optic nerves/group, -way ANOVA, $^{**}P < 0.01$, $^{***}P < 0.001$, $^{****}P < 0.0001$.

Investigative Ophthalmology & Visual Science

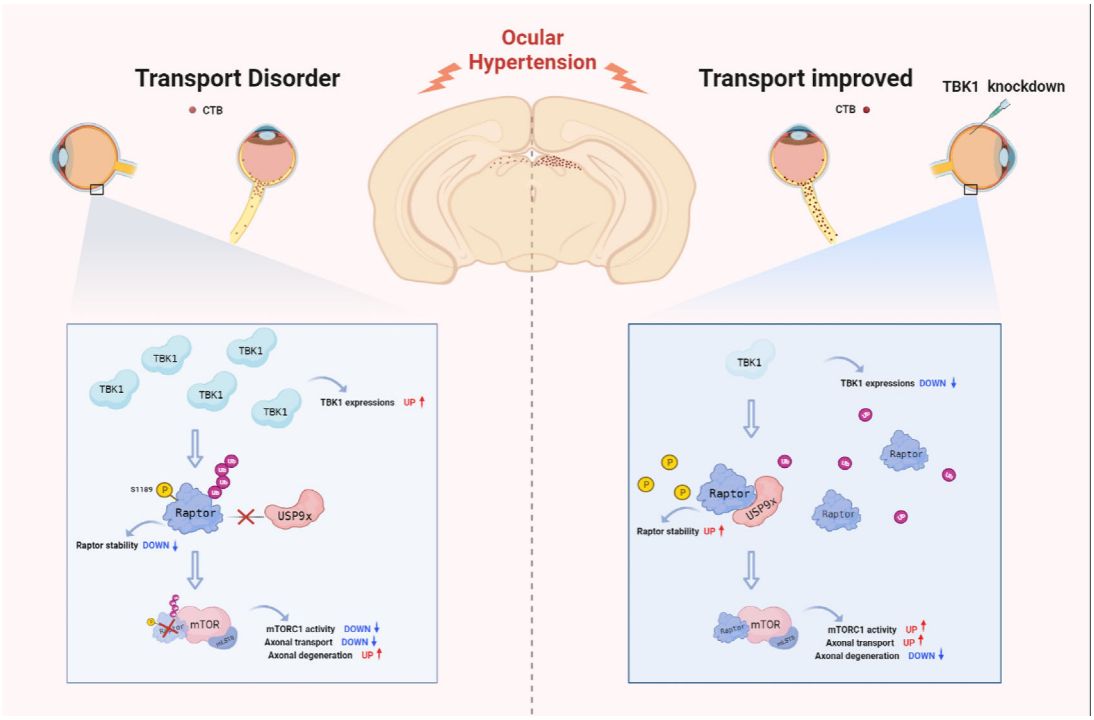

Figure 9. Schematic illustrating the mechanism that TBK1 knockdown improved RGCs axonal transport by activating mTORC1 signaling. In response to acute ocular hypertension, the expression levels of TBK1 in RGC are upregulated. TBK1 increases the phosphorylation of RAPTOR on Ser1189, which hinders the combination of RAPTOR and USP9X, leading to an increase in RAPTOR ubiquitination and the decline of protein stabilization. Subsequently, RAPTOR degradation inhibits the mTORC1 signaling pathway, resulting in axonal transport deficits and neurodegeneration. Thus, TBK1 knockdown might alleviate neuronal injury via the activation of mTORC1 signaling pathway in glaucoma.

yet been elucidated. Many studies have focused on the recognized interaction between TBK1 and OPTN, another glaucoma-associated protein, which mediates autophagy-dependent pathological processes.[42,43] The M98K-OPTN mutation has been reported to activate TBK1, which in turn enhances OPTN phosphorylation at Ser177 and induces autophagic flux and retinal cell death.[44] Another study reported that the E50K-OPTN mutation strongly interacts with TBK1 and mediates glaucomatous phenotypes.[45] In addition to OPTN-related mechanisms, TBK1 has been reported to participate in other mechanisms of neural injury. For example, TBK1 regulated the expression of p16 and induced RGC senescence in retinal ischemic injury. TBK1 also phosphorylates tau and enhances its neurotoxicity, which induces subsequent neurodegeneration in Alzheimer's disease.[46] Here, we identified an interaction between TBK1 and mTORC1, which is a crucial signaling hub related to neural function.[15] Our experimental results showed that TBK1 is a negative regulator of mTORC1 and that inhibition of mTORC1 counteracts the neuroprotective effect exerted by TBK1 knockdown.

The role of mTORC1 in retinal development and optic nerve protection has been widely investigated.[47,48] An immunohistological study confirmed that the components of the mTORC1 pathway were predominantly distributed in RGCs and their axons.[49] The mTORC1 regulates mRNA translation and protein synthesis in neurons, which controls neuronal development, synaptic plasticity and axon guidance.[50-54] The mTORC1 also participates in autophagy, which underlies neurodegenerative diseases, such as glaucoma.[55,56] Multiple signals and molecules exerting neuroprotective effects depend on mTORC1 activation. For example, HDAC5 promotes optic nerve regeneration by activating the mTORC1 pathway.[57] Lin28a attenuates cerebral ischemia/reperfusion injury through Sirt3-mediated mTORC1 activation.[58] In our study, we demonstrated mTORC1-dependent neuroprotective effects downstream of knocked down TBK1 in a retinal damage model.

Several studies have reported an interaction between TBK1 and mTORC1. However, the results of these studies were not identical, as they depended on different cellular contexts. Antonia et al. found that TBK1 suppressed mTORC1 activity through phosphorylation of RAPTOR at Ser877.[24] However, this study did not elucidate how phosphorylation of RAPTOR at Ser877 inhibited mTORC1 activation. In the present study, we identified a degradation-related phosphorylation site of RAPTOR at Ser1189, which was phosphorylated by TBK1 and negatively influenced the stability of RAPTOR, leading to mTORC1 inactivation. In our study, we used two post-translational modification databases to predict potential sites of TBK1 phosphorylation of RAPTOR. The Group Based Prediction System identified a characteristic motif of TBK1 phosphorylation substrates in RAPTOR, whereas the PhosphoSitePlus database provided phosphorylation sites of RAPTOR that had been reported in mass spectrometry studies. The intersection of the results of these two databases ensured the kinase specificity as well as confirmed the authenticity of the predicted sites. The results included the Ser877 site reported in the abovementioned article, which might be partially involved in TBK1-mediated inhibition of the mTORC1 pathway. Notably, our study identified another phosphorylation site in RAPTOR and

Investigative Ophthalmology & Visual Science

demonstrated a novel mechanism underlying the negative regulation of mTORC1 by TBK1. Moreover, TBK1 has been previously reported to inhibit mTORC1 signaling in prostate cancer (PCa) cells and the regulate the dormancy and drug resistance in PCa.[59] TBK1 also suppressed mTORC1 activity in an autoimmune/autoinflammatory disease mouse model, leading to dysregulated cellular metabolism.[26] These studies support the results indicating that TBK1 functions as an upstream negative regulator of mTORC1 but do not shed light on the specific mechanisms. Our study might help provide insights to explain these phenotypes. In contrast, some other studies have reported that TBK1 promoted mTORC1 activation. Cagri Bodur et al. found that TBK1 phosphorylated mTOR at Ser2159 and activated mTORC1 in response to growth factors and innate immune agonists.[25] Another study reported that TBK1 mediated growth factor-stimulated mTORC1 activation in a mouse model of lung cancer.[60] These different outcomes may have been due to different cellular states and pathological processes, and different molecular mechanisms are probably mutually balanced.

We showed that the phosphorylation-dependent degradation of RAPTOR was associated with the deubiquitinating enzyme USP9X. A previous study had reported that USP9X maintains the RAPTOR protein level during neural development.[34] The mechanism of this modulatory effect and its significance under pathological conditions have not yet been elucidated. USP9X plays an important role in regulating neural function and development.[61-64] As a substrate-specific deubiquitylating enzyme, USP9X deubiquitinates neuromodulators to maintain their stability and is indirectly involved in neural function modulation.[65,66] In addition, a study has reported that mTORC2 activity is regulated by the USP9X-mediated deubiquitination of RICTOR,[67] but the interaction between USP9X and mTORC1 had not been discussed to date. Post-translational modifications (PTMs) are generally involved in the regulation of mTORC1 activity. AMPK mediates RAPTOR phosphorylation at Ser722 and Ser792, leading to suppressed mTORC1 activity combination with 14-3-3.[68] PKA phosphorylates RAPTOR at Ser791, inhibiting mTORC1.[69] In this study, we found another phosphorylation site in RAPTOR that negatively regulated mTORC1. Ser1189 is an evolutionally conserved residue located in the WD40 region of RAPTOR, and it has been reported to be associated with ubiquitin-dependent proteolysis.[70] We found that phosphorylation of RAPTOR at Ser1189 impeded the binding of RAPTOR to USP9X, possibly due to conformational changes induced by phosphorylation. However, to identify the precise binding sites in these two proteins and the specific regulatory mechanisms involved, further exploration is needed.

Because of the difficulties in the extraction and culture of primary RGCs, this study used SH-SY5Y cells, which have some similarity to RGCs, to mimic cultured neurons in vitro to perform phenotypic experiments to verify the neuroprotective effects of the molecule. This is a limitation of the present study.

Conclusions

We demonstrated that TBK1 knockdown in RGCs increased axonal transport and protected against axonal degeneration in a mouse model of glaucoma induced by AOHT. Loss of TBK1 led to neuroprotective effects mediated through activation of the mTORC1 pathway. We elucidated a novel mechanism by which TBK1 phosphorylates RAPTOR at serine residue 1189 and mediates its degradation via the ubiquitin–proteasome, thus impeding mTORC1 activation. In depth, phosphorylation of RAPTOR at Ser1189 blocked its interaction with the deubiquitinating enzyme USP9X, leading to increased ubiquitination and reduced protein stability (Fig. 9).

The mechanisms and interventions of RGC damage have been extensively explored. Our study identified a novel mechanism involved in the interaction between the glaucoma risk gene *TBK1* and the pivotal mTORC1 pathway and may lead to the identification of new therapeutic targets in glaucoma and other neurodegenerative diseases.

Acknowledgments

Supported by funding from the National Natural Science Foundation of China Grant no. 82070965 (to Hong Zhang) and Tongji Hospital (HUST) Foundation for Excellent Young Scientist Grant No. 2020YQ18 (to Yin Zhao).

Author Contributions: Meng Ye, Hong Zhang, and Yin Zhao designed the research. Yuanyuan Hu conducted the experiments and acquired the data. Bowen Zhao and Qianxue Mou analyzed the data. Yueqi Ni, Jing Luo, and Lu Li wrote the manuscript.

Availability of Data and Materials: In this study, the original contributions are included in the article, and further inquiries can contact the corresponding author directly.

Disclosure: **M. Ye**, None; **Y. Hu**, None; **B. Zhao**, None; **Q. Mou**, None; **Y. Ni**, None; **J. Luo**, None; **L. Li**, None; **H. Zhang**, None; **Y. Zhao**, None

References

1. Weinreb RN, Aung T, Medeiros FA. The pathophysiology and treatment of glaucoma: a review. *JAMA*. 2014;311(18):1901–1911.
2. De Moraes CG, Liebmann JM, Levin LA. Detection and measurement of clinically meaningful visual field progression in clinical trials for glaucoma. *Prog Retin Eye Res*. 2017;56:107–147.
3. Stein JD, Khawaja AP, Weizer JS. Glaucoma in adults-screening, diagnosis, and management: a review. *JAMA*. 2021;325(2):164–174.
4. Killer HE, Pircher A. Normal tension glaucoma: review of current understanding and mechanisms of the pathogenesis. *Eye (Lond)*. 2018;32(5):924–930.
5. Gordon MO, Kass MA. What we have learned from the ocular hypertension treatment study. *Am J Ophthalmol*. 2018;189:xxiv–xxvii.
6. Guymer C, Wood JP, Chidlow G, Casson RJ. Neuroprotection in glaucoma: recent advances and clinical translation. *Clinic Exp Ophthalmol*. 2019;47(1):88–105.
7. Fingert JH, Robin AL, Stone JL, et al. Copy number variations on chromosome 12q14 in patients with normal tension glaucoma. *Hum Mol Genet*. 2011;20(12):2482–2494.
8. Kawase K, Allingham RR, Meguro A, et al. Confirmation of TBK1 duplication in normal tension glaucoma. *Exp Eye Res*. 2012;96(1):178–180.
9. Fingert JH, Miller K, Hedberg-Buenz A, et al. Transgenic TBK1 mice have features of normal tension glaucoma. *Hum Mol Genet*. 2017;26(1):124–132.
10. Fitzgerald KA, McWhirter SM, Faia KL, et al. IKKepsilon and TBK1 are essential components of the IRF3 signaling pathway. *Nat Immunol*. 2003;4(5):491–496.

11. Wei X, Cho KS, Thee EF, Jager MJ, Chen DF. Neuroinflammation and microglia in glaucoma: time for a paradigm shift. *J Neurosci Res*. 2019;97(1):70–76.
12. Herhaus L. TBK1 (TANK-binding kinase 1)-mediated regulation of autophagy in health and disease. *Matrix Biol: J International Society for Matrix Biology*. 2021;100-101:84–98.
13. Fingert JH, Darbro BW, Qian Q, et al. TBK1 and flanking genes in human retina. *Ophthalmic Genet*. 2014;35(1):35–40.
14. Switon K, Kotulska K, Janusz-Kaminska A, Zmorzynska J, Jaworski J. Molecular neurobiology of mTOR. *Neuroscience*. 2017;341:112–153.
15. Swiech L, Perycz M, Malik A, Jaworski J. Role of mTOR in physiology and pathology of the nervous system. *Biochim Biophys Acta*. 2008;1784(1):116–132.
16. Rao YQ, Zhou YT, Zhou W, Li JK, Li B, Li J. mTORC1 activation in Chx10-SPECIFIC Tsc1 knockout mice accelerates retina aging and degeneration. *Oxid Med Cell Longev*. 2021;2021:6715758.
17. Lim S, Kim YJ, Park S, et al. mTORC1-induced retinal progenitor cell overproliferation leads to accelerated mitotic aging and degeneration of descendent Müller glia. *Elife*. 2021;10:e70079.
18. Sethna S, Scott PA, Giese APJ, et al. CIB2 regulates mTORC1 signaling and is essential for autophagy and visual function. *Nat Commun*. 2021;12(1):3906.
19. Yang X, Hondur G, Li M, et al. Proteomics analysis of molecular risk factors in the ocular hypertensive human retina. *Invest Ophthalmol Vis Sci*. 2015;56(10):5816–5830.
20. Belforte N, Agostinone J, Alarcon-Martinez L, et al. AMPK hyperactivation promotes dendrite retraction, synaptic loss, and neuronal dysfunction in glaucoma. *Molec Neurodegen*. 2021;16(1):43.
21. Ye M, Huang J, Mou Q, et al. CD82 protects against glaucomatous axonal transport deficits via mTORC1 activation in mice. *Cell Death Dis*. 2021;12(12):1149.
22. Agostinone J, Alarcon-Martinez L, Gamlin C, Yu WQ, Wong ROL, Di Polo A. Insulin signalling promotes dendrite and synapse regeneration and restores circuit function after axonal injury. *Brain: a JNeurol*. 2018;141(7):1963–1980.
23. Liu K, Qiu D, Liang X, et al. Lipotoxicity-induced STING1 activation stimulates mTORC1 and restricts hepatic lipophagy. *Autophagy*. 2022;18(4):860–876.
24. Antonia RJ, Castillo J, Herring LE, et al. TBK1 limits mTORC1 by promoting phosphorylation of RAPTOR Ser877. *Sci Rep*. 2019;9(1):13470.
25. Bodur C, Kazyken D, Huang K, et al. The IKK-related kinase TBK1 activates mTORC1 directly in response to growth factors and innate immune agonists. *The EMBO J*. 2018;37(1):19–38.
26. Hasan M, Gonugunta VK, Dobbs N, et al. Chronic innate immune activation of TBK1 suppresses mTORC1 activity and dysregulates cellular metabolism. *Proc Natl Acad Sci USA*. 2017;114(4):746–751.
27. Park TS, Bhutto I, Zimmerlin L, et al. Vascular progenitors from cord blood-derived induced pluripotent stem cells possess augmented capacity for regenerating ischemic retinal vasculature. *Circulation*. 2014;129(3):359–372.
28. Gao G, Oda Y, Wei EP, Povlishock JT. The adverse pial arteriolar and axonal consequences of traumatic brain injury complicated by hypoxia and their therapeutic modulation with hypothermia in rat. *J Cereb Blood Flow Metab*. 2010;30(3):628–637.
29. Weinreb RN, Leung CK, Crowston JG, et al. Primary open-angle glaucoma. *Nat Rev Dis Primers*. 2016;2:16067.
30. Maia PD, Hemphill MA, Zehnder B, Zhang C, Parker KK, Kutz JN. Diagnostic tools for evaluating the impact of focal axonal swellings arising in neurodegenerative diseases and/or traumatic brain injury. *J Neurosci Methods*. 2015;253:233–243.
31. Crish SD, Sappington RM, Inman DM, Horner PJ, Calkins DJ. Distal axonopathy with structural persistence in glaucomatous neurodegeneration. *Proc Natl Acad Sci USA*. 2010;107(11):5196–5201.
32. Stekic A, Zeljkovic M, Zaric Kontic M, et al. Intermittent theta burst stimulation ameliorates cognitive deficit and attenuates neuroinflammation via PI3K/Akt/mTOR signaling pathway in Alzheimer's-like disease model. *Front Aging Neurosci*. 2022;14:889983.
33. Fang C, Bourdette D, Banker G. Oxidative stress inhibits axonal transport: implications for neurodegenerative diseases. *Molec Neurodegen*. 2012;7:29.
34. Bridges CR, Tan MC, Premarathne S, et al. USP9X deubiquitylating enzyme maintains RAPTOR protein levels, mTORC1 signalling and proliferation in neural progenitors. *Sci Rep*. 2017;7(1):391.
35. Stegeman S, Jolly LA, Premarathne S, et al. Loss of Usp9x disrupts cortical architecture, hippocampal development and TGFβ-mediated axonogenesis. *PLoS One*. 2013;8(7):e68287.
36. Yoon S, Parnell E, Kasherman M, et al. Usp9X controls ankyrin-repeat domain protein homeostasis during dendritic spine development. *Neuron*. 2020;105(3):506–521.e7.
37. Ritch R, Darbro B, Menon G, et al. TBK1 gene duplication and normal-tension glaucoma. *JAMA Ophthalmol*. 2014;132(5):544–548.
38. Ahmad L, Zhang SY, Casanova JL, Sancho-Shimizu V. Human TBK1: a gatekeeper of neuroinflammation. *Trends Molec Med*. 2016;22(6):511–527.
39. Oakes JA, Davies MC, Collins MO. TBK1: a new player in ALS linking autophagy and neuroinflammation. *Molec Brain*. 2017;10(1):5.
40. Mathur V, Burai R, Vest RT, et al. Activation of the STING-dependent type I interferon response reduces microglial reactivity and neuroinflammation. *Neuron*. 2017;96(6):1290–1302.e6.
41. Xu D, Jin T, Zhu H, et al. TBK1 suppresses RIPK1-driven apoptosis and inflammation during development and in aging. *Cell*. 2018;174(6):1477–1491.e19.
42. Minegishi Y, Nakayama M, Iejima D, Kawase K, Iwata T. Significance of optineurin mutations in glaucoma and other diseases. *Prog Retin Eye Res*. 2016;55:149–181.
43. Li F, Xie X, Wang Y, et al. Structural insights into the interaction and disease mechanism of neurodegenerative disease-associated optineurin and TBK1 proteins. *Nat Commun*. 2016;7:12708.
44. Sirohi K, Kumari A, Radha V, Swarup G. A glaucoma-associated variant of optineurin, M98K, activates Tbk1 to enhance autophagosome formation and retinal cell death dependent on Ser177 phosphorylation of optineurin. *PLoS One*. 2015;10(9):e0138289.
45. Medchalmi S, Tare P, Sayyad Z, Swarup G. A glaucoma- and ALS-associated mutant of OPTN induces neuronal cell death dependent on Tbk1 activity, autophagy and ER stress. *The FEBS J*. 2021;288(15):4576–4595.
46. Abreha MH, Ojelade S, Dammer EB, et al. TBK1 interacts with tau and enhances neurodegeneration in tauopathy. *J Biolog Chem*. 2021;296:100760.
47. Choi JH, Jo HS, Lim S, et al. mTORC1 accelerates retinal development via the immunoproteasome. *Nat Commun*. 2018;9(1):2502.
48. Leibinger M, Andreadaki A, Fischer D. Role of mTOR in neuroprotection and axon regeneration after inflammatory stimulation. *Neurobiol Dis*. 2012;46(2):314–324.

Investigative Ophthalmology & Visual Science

49. Losiewicz MK, Elghazi L, Fingar DC, et al. mTORC1 and mTORC2 expression in inner retinal neurons and glial cells. *Exp Eye Res*. 2020;197:108131.
50. Morita T, Sobue K. Specification of neuronal polarity regulated by local translation of CRMP2 and Tau via the mTOR-p70S6K pathway. *J Biologic Chem*. 2009;284(40):27734–27745.
51. Kim SG, Lee S, Kim Y, et al. Tanc2-mediated mTOR inhibition balances mTORC1/2 signaling in the developing mouse brain and human neurons. *Nat Commun*. 2021;12(1):2695.
52. Takei N, Nawa H. mTOR signaling and its roles in normal and abnormal brain development. *Front Molecul Neurosci*. 2014;7:28.
53. Sun J, Liu Y, Jia Y, et al. UBE3A-mediated p18/LAMTOR1 ubiquitination and degradation regulate mTORC1 activity and synaptic plasticity. *eLife*. 2018;7:e37993.
54. Gong X, Zhang L, Huang T, et al. Activating the translational repressor 4E-BP or reducing S6K-GSK3β activity prevents accelerated axon growth induced by hyperactive mTOR in vivo. *Hum Mol Genet*. 2015;24(20):5746–5758.
55. Rabanal-Ruiz Y, Otten EG, Korolchuk VI. mTORC1 as the main gateway to autophagy. *Essays in Biochem*. 2017;61(6):565–584.
56. Ishikawa M, Takaseki S, Yoshitomi T, Covey DF, Zorumski CF, Izumi Y. The neurosteroid allopregnanolone protects retinal neurons by effects on autophagy and GABRs/GABA(A) receptors in rat glaucoma models. *Autophagy*. 2021;17(3):743–760.
57. Pita-Thomas W, Mahar M, Joshi A, Gan D, Cavalli V. HDAC5 promotes optic nerve regeneration by activating the mTOR pathway. *Exp Neurol*. 2019;317:271–283.
58. Chen D, Zheng K, Wu H, et al. Lin28a attenuates cerebral ischemia/reperfusion injury through regulating Sirt3-induced autophagy. *Brain Res Bull*. 2021;170:39–48.
59. Kim JK, Jung Y, Wang J, et al. TBK1 regulates prostate cancer dormancy through mTOR inhibition. *Neoplasia*. 2013;15(9):1064–1074.
60. Zhu L, Li Y, Xie X, et al. TBKBP1 and TBK1 form a growth factor signalling axis mediating immunosuppression and tumourigenesis. *Nat Cell Biol*. 2019;21(12):1604–1614.
61. Oishi S, Premarathne S, Harvey TJ, et al. Usp9x-deficiency disrupts the morphological development of the postnatal hippocampal dentate gyrus. *Sci Rep*. 2016;6:25783.
62. Rott R, Szargel R, Haskin J, et al. α-Synuclein fate is determined by USP9X-regulated monoubiquitination. *Proc Natl Acad Sci USA*. 2011;108(46):18666–18671.
63. Paemka L, Mahajan VB, Ehaideb SN, et al. Seizures are regulated by ubiquitin-specific peptidase 9 X-linked (USP9X), a de-ubiquitinase. *PLoS Genet*. 2015;11(3):e1005022.
64. Johnson BV, Kumar R, Oishi S, et al. Partial loss of USP9X function leads to a male neurodevelopmental and behavioral disorder converging on transforming growth factor β signaling. *Biologic Psychiatry*. 2020;87(2):100–112.
65. Yoon S, Parnell E, Penzes P. TGF-β-induced phosphorylation of Usp9X stabilizes ankyrin-G and regulates dendritic spine development and maintenance. *Cell Rep*. 2020;31(8):107685.
66. Han KJ, Foster DG, Zhang NY, et al. Ubiquitin-specific protease 9x deubiquitinates and stabilizes the spinal muscular atrophy protein-survival motor neuron. *J Biologic Chem*. 2012;287(52):43741–43752.
67. Wrobel L, Siddiqi FH, Hill SM, et al. mTORC2 assembly is regulated by USP9X-mediated deubiquitination of RICTOR. *Cell Rep*. 2020;33(13):108564.
68. Gwinn DM, Shackelford DB, Egan DF, et al. AMPK phosphorylation of RAPTOR mediates a metabolic checkpoint. *Molec Cell*. 2008;30(2):214–226.
69. Jewell JL, Fu V, Hong AW, et al. GPCR signaling inhibits mTORC1 via PKA phosphorylation of Raptor. *eLife*. 2019;8:e43038.
70. Ghosh P, Wu M, Zhang H, Sun H. mTORC1 signaling requires proteasomal function and the involvement of CUL4-DDB1 ubiquitin E3 ligase. *Cell Cycle (Georgetown, Tex)*. 2008;7(3):373–381.

Investigative Ophthalmology & Visual Science